# NOVEL FLAT INTERFACE NERVE ELECTRODE (FINE) DESIGN BY ELECTRICALLY DRIVEN SHAPE MEMORY ALLOYS (SMAs)

by

**Abdülsamet Şahin**

B.S., in Biology, Fatih University, 2014

B.S., in Electrical and Electronic Engineering, Fatih University, 2015

Submitted to the Institute of Biomedical Engineering

in partial fulfillment of the requirements

for the degree of

Master of Science

in

Biomedical Engineering

Boğaziçi University

2019

# NOVEL FLAT INTERFACE NERVE ELECTRODE (FINE) DESIGN BY ELECTRICALLY DRIVEN SHAPE MEMORY ALLOYS (SMAs)

## APPROVED BY:

Assoc. Prof. Dr. Özgür Kocatürk .....
(Thesis Advisor)

Prof. Dr. Burak Güçlü .....
(Thesis Co-advisor)

Assoc. Prof. Dr. Bora Garipcan .....

Assoc. Prof. Dr. Esin Öztürk Işık .....

Prof. Dr. Kürşat Kazmanlı .....

**DATE OF APPROVAL:** 30 July 2019

# ACKNOWLEDGMENTS

I would like to thank my advisors Dr. Özgür Kocatürk and Dr. Burak Güçlü for their constant and invaluable help. Through the learning process of this thesis, they guided me in the right direction whenever they thought I need it.

I would also like to acknowledge Ahmet Turan Talaş for his contributions to my study. When I looked for an alternative solution to advance my research, he showed me different perspectives.

Morteza Teymoori is kindly acknowledged for offering his endless help.

Finally, I want to thank my family, for they have always encouraged me to realize my dreams.

# ACADEMIC ETHICS AND INTEGRITY STATEMENT

I, Abdülsamet Şahin, hereby certify that I am aware of the Academic Ethics and Integrity Policy issued by the Council of Higher Education (YÖK) and I fully acknowledge all the consequences due to its violation by plagiarism or any other way.

Name :

Signature:

Date:

# ABSTRACT

## NOVEL FLAT INTERFACE NERVE ELECTRODE (FINE) DESIGN BY ELECTRICALLY DRIVEN SHAPE MEMORY ALLOYS (SMAs)

Flat Interface Nerve Electrodes (FINE) reshape the nerve, which results in an oval geometry and causes the fascicles to be arranged on an axis. In this way, they can provide selectivity at the fascicle level without penetrating the nerve. However, the constant pressure exerted on the nerve during the reshaping process causes nerve damage. Therefore, a dynamic design is required to apply the required force for shaping the nerve when excitation or receiving signal is necessary. The aim of this study is to design a dynamic FINE that can apply gradual pressure on the nerve using shape memory alloys (SMA). In this study, the actuation mechanism that will apply pressure on the nerve is provided with a SMA shaped as a spring. The main frame of the electrode was fabricated with a 3D printer. Electrode contacts were produced with chromium and gold coated with PVD technique on polyimide. The overall design performance was evaluated by a forcemeter. As a result of driving the actuator with various current values, it has been proved that it can perform gradual and controlled compression. In addition, the actuator can produce up to 0.7 N force. This demonstrates that this design can be used in the manufacture of an electrode capable of gradual compression, as well as in a system designed to cause controlled damage to the nerves.

**Keywords:** Shape Memory Alloy (SMA), Flat Interface Nerve Electrode (FINE), Actuator.

# ÖZET

## ELEKTRİK KONTROLLÜ ŞEKİL HAFIZALI ALAŞIMLAR (ŞHA) İLE YENİ DÜZ ARAYÜZ SİNİR ELEKTROTU (DASE) TASARIMI

Düz Arayüz Sinir Elektrotlar (DASE) sinir üzerinde meydana getirdikleri yeniden şekillendirme sonucunda onları oval bir forma kavuşturmakta ve fasiküllerin bir eksende dizilmelerine neden olmaktadır. Bu sayede sinire penetre olmadan fasikül düzeyinde seçicilik sağlayabilmektedirler. Bununla birlikte, yeniden şekillendirme sürecinde sinir üzerine uygulanan basınç sinirde hasara sebep olmaktadır. Bu sebeple sinirde hasara sebep olmadan şekillendirme için gerekli kuvveti uygulayabilecek dinamik bir tasarım gerekmektedir. Bu çalışmanın amacı şekil hafızalı metaller kullanarak sinir üzerine kademeli basınç uygulayabilecek dinamik bir düz arayüz sinir elektrotu tasarlamaktır. Bu çalışmada sinir üzerine basınç uygulayacak hareket mekanizması yay olarak şekillendirilen hafızalı metal ile sağlanmıştır. Elektrotun ana çerçevesinin üretimi 3D yazıcı ile oluşturulmuştur. Siniri stimüle edecek kontaklar ise polyimide film üzerine PVD yöntemiyle kaplanan krom ve altın ile sağlanmıştır. Tasarımın başarısı kuvvet ölçer ile değerlendirilmiştir. Üretilen elektrotun farklı akım değerleri ile uyarılması sonucunda kademeli ve kontrollü sıkıştırma yapabildiği yapılan testler ile kanıtlanmıştır. Ayrıca imal edilen aktüatör 0.7 N a kadar kuvvet üretebilmektedir. Bu göstermektedir ki bu tasarım kademeli sıkıştırma yapabilen bir elektrot yapımında kullanılabileceği gibi aynı zamanda sinirlere kontrollü hasar vermek amacıyla tasarlanacak sistemlerde de kullanılabilecek bir araçtır.

**Anahtar Şözcükler:** Şekil Hafızalı Alaşım (ŞHA), Düz Arayüz Sinir elektrotu (DASE), Aktüatör.

# TABLE OF CONTENTS

# LIST OF FIGURES

# LIST OF TABLES

# LIST OF SYMBOLS

| | |
|---|---|
| MPa | Mega Pascal |
| MHz | Mega Hertz |
| g | Gram |
| $\mu m$ | Micrometer |
| nm | Nanometer |
| J/Kg | Joules per Kilograms |
| $MJ/m^3$ | Megajoules per cubic meter |
| °C | Degree Centigrade |
| $A_s$ | Austenite start temperature |
| $A_f$ | Austenite finish temperature |
| $M_s$ | Martensite start temperature |
| $M_f$ | Martensite finish temperature |
| $\varepsilon_t$ | Transformation strain |
| $\sigma_s^A$ | Austenite start stress |
| $\sigma_f^A$ | Austenite finish stress |
| $\sigma_s^M$ | Martensite start stress |
| $\sigma_f^M$ | Martensite finish stress |
| $\sigma$ | Stress |
| $\varepsilon$ | Strain |
| T | Temperature |
| GPa | Gigapascal |
| Pa | Pascal |
| mg | Milligrams |
| mmHg | Millimeter of mercury |
| ° C/min | Degrees centigrade per minutes |
| %W/V | Weight per Volume concentration |
| V | Volts |
| $M\Omega$ | Megaohm |

| | |
|---|---|
| A | Amperes |
| ms | Milliseconds |

# LIST OF ABBREVIATIONS

| | |
|---|---|
| BFR | Bend and Free Recovery |
| CAD | Computer Aided Design |
| DSC | Differential Calorimetric Spectroscopy |
| DC | Direct Current |
| FEM | Finite Element Method |
| FINE | Flat Interface Nerve Electrode |
| LPS | Lower Plateau Stress |
| Md | Martensite Deformation |
| MOSFET | Metal-Oxide-Semiconductor Field-Effect Transistor |
| NiTi | Nitinol |
| PNE | Peripheral Nerve Electrode |
| PDMS | Polydimethylsiloxane |
| PI | Polyimide |
| PCB | Printed Circuit Board |
| SM | Shape Memory |
| SMA | Shape Memory Alloy |
| SME | Shape Memory Effect |
| SIM | Stress Induced Martensite |
| UPS | Upper Plateau Stress |
| UV | Ultra Violet |

# 1. INTRODUCTION

## 1.1 Shape Memory Alloys

In 1932, when the shape recovery feature of inelastic-deformed Au-Cd alloy by temperature was first discovered, people were far from understanding the importance of this development, and so the discovery did not attract enough attention. In the following years, similar properties were observed in various alloys such as CuZn. In 1961, the equiatomic alloy of nickel and titanium, later called Nitinol, was discovered.

The relatively easy and cost-effective production and processability of nitinol has led SMA to come to the fore again. Today, SMAs are used on a wide scale from aviation industry to medical stent applications.

### 1.1.1 Physics of SMAs

SMAs exhibit two different crystal structures: martensite and austenite. Martensite is the low temperature phase of the alloy and has a B19' monoclinic crystal structure. Austenite is the high temperature phase and has a B2 crystal structure.

### 1.1.2 Phase Transformation

The crystal lattice geometry of an SMA is determined by temperature and stress. When an SMA with twinned martensite crystal structure is subjected to a certain amount of stress, inelastic deformations occur in the crystal structure and the structure is hereinafter referred to as detwinned martensite.

This structure converts to austenite form when the required heat energy is given to the SMA. However, with the drop in the heat, austenite phase turns back into the

former twinned martensite form. These phase changes shown by SMAs are an example of diffusionless solid state phase change [1].

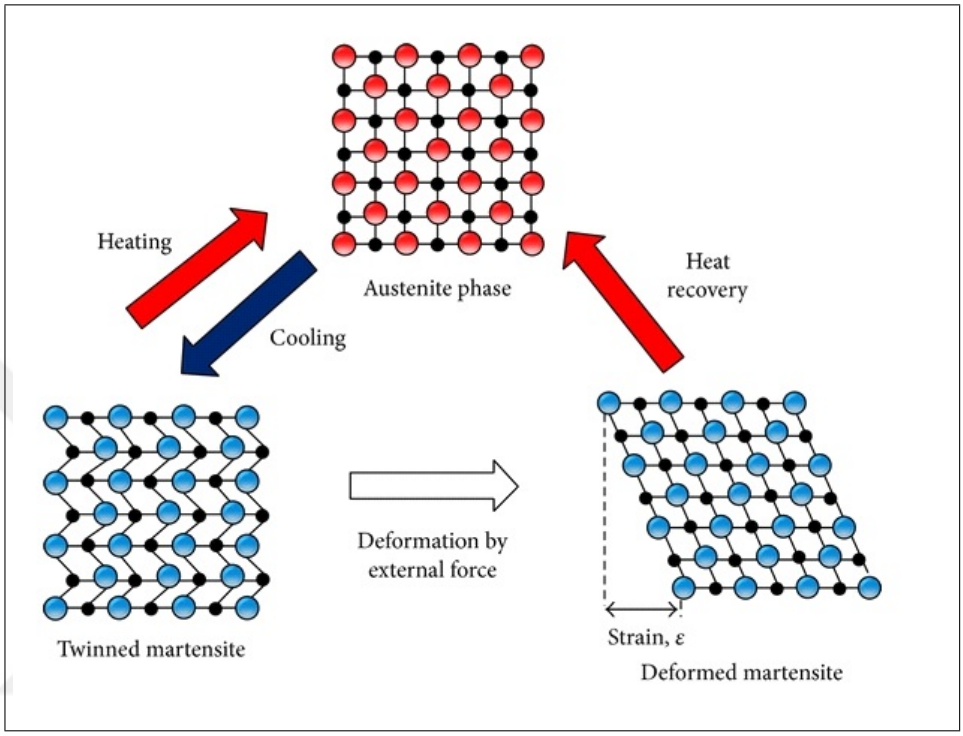


**Figure 1.1** Phase transformation of a SMA in crystal structure [2].

Figure 1.1 shows the macroscopic changes of an SMA sample under certain stress due to phase change as a result of temperature change.

Under certain stress, the detwinned-martensite crystal structure of the SMA starts to change the lattice configuration by reaching the temperature austenite start ($A_s$) point, and when the temperature reaches the austenite finish ($A_f$) value, the final form, austenite crystal structure (B2), is formed. As the temperature begins to fall, no change in the crystal structure is observed until the martensite start ($M_s$) point. After this value, the SMA sample begins to move to the detwinned-martensite crystal structure and after the martensite finish ($M_f$) temperature it becomes completely detwinned-martensite.

The transformation between the martensite and austenite phases takes place

at different temperatures. This difference, called thermal hysteresis, is indicated by ΔT. Hysteresis values of SMAs vary according to the element they contain and the production processes they are exposed to.

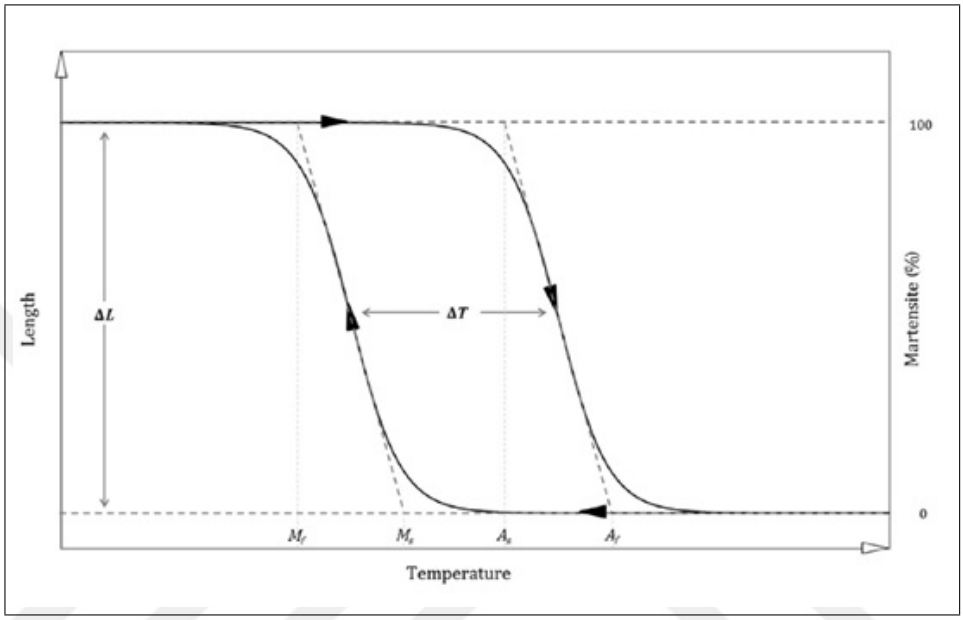


**Figure 1.2** Transformation vs temperature curve for a specimen under constant stress being cooled and heated. ΔT: Transformation hysteresis; $M_s$: Martensite start; $M_f$: Martensite finish; $A_s$: Austenite start and $A_f$: Austenite finish [3].

### 1.1.3 Shape Memory Effect (SME)

Shape memory effect (SME) is a term used to describe a specific material's ability to recover its original form with temperature elevation after an inelastic deformation. This is a manifestation of reversible thermoelastic martensitic transformation in which the crystal structure of the material is altered. Figure 1.3 shows an SME behavior exhibited by an SMA that is exposed to stress and temperature changes. In part A of the figure, the twinned-martensite crystal form is subjected to stress loading under constant temperature. With the increasing stress, inelastic deformations occurred in the material structure and the crystal order turned into detwinned-martensite form. Even if the applied load is removed, the material cannot regain its original form. Part B shows the application of temperature to alloy in the form of detwinned martensite

under zero stress. With the applied temperature, the crystal geometry has reached the austenite configuration. In this way, the material has returned to its first form in size and shape. Section C shows the conversion of austenite to twinned martensite, which does not cause macroscopic change of the alloy, resulting from removing of temperature application.The SME behavior of SMAs is critical for the production of externally-induced smart actuators in small size.

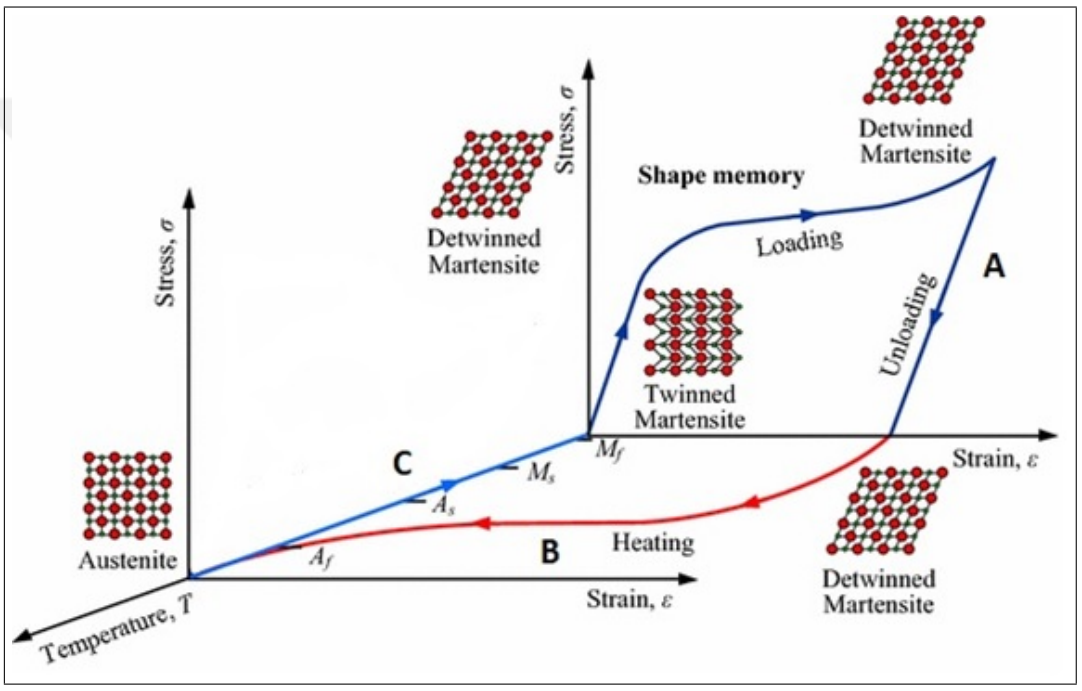


**Figure 1.3** Shape Memory Effect behavior of an SMA according to stress and temperature conditions. Adapted from [Seismic behavior of self-centering reinforced concrete wall enabled by superelastic shape memory alloy bars [4].

### 1.1.4 Pseudoelasticity or Superelasticity

Superelasticity or Pseudoelasticity is a unique feature of SMAs at temperatures above $A_f$. If sufficient stress is applied to an SMA at a temperature above $A_f$ degree, austenite configuration of the structure changes to martensite form called stress induced martensite (SIM). However, this is a temporary condition, the SMA regains its austenite crystal structure with removal of stress applied. This stress-related phase transformation, which occurs at temperature above $A_f$, is called superelasticity. This

phenomenon is usually characterized by cyclic tensile test.

Figure 1.4 shows the stress-dependent changes of an SMA over the $A_f$ temperature. Stress loading to an SMA in the form of austenite first causes elastic deformation (A-B). When the Upper Plateau Stress (UPS) value is exceeded, the transition from the austenite phase structure to the detwinned martensite structure and the corresponding macro scale shape changes are observed (B-C). Continued stress increase causes elastic deformation of the martensite form (C-D) After this point, the structure begins to return to its former form with the reduction of applied stress to the sample. However, no significant strain change is observed until the Lower Plateau Stress (LPS) value. With complete removal of applied stress, alloy returns to the initial austenite structure without residual strain. There is a difference between the UPS and LPS values, which is called mechanical hysteresis, due to the degradation and friction in the crystal structure.

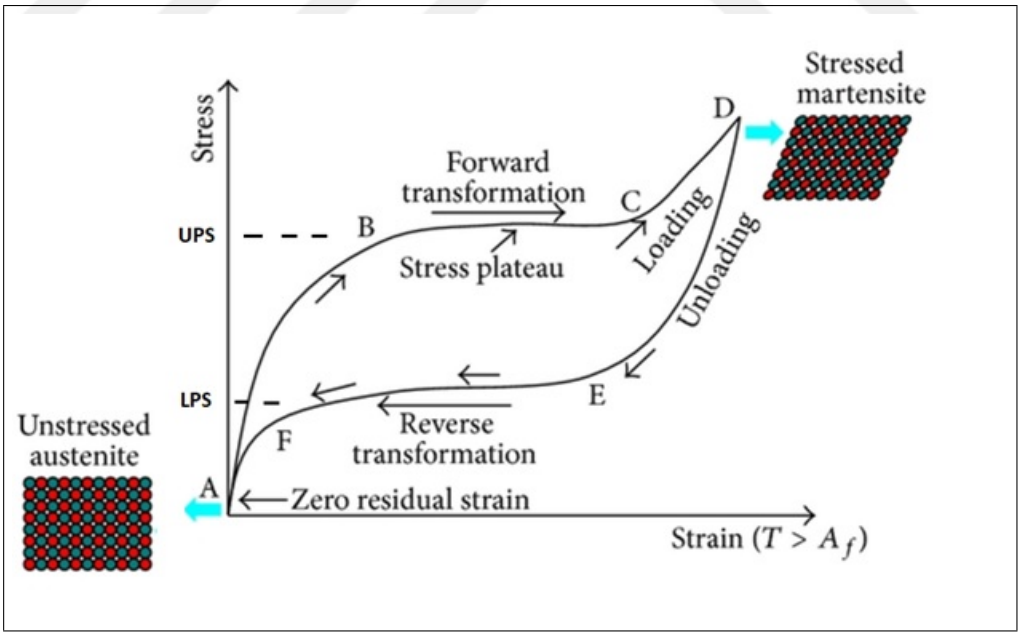


**Figure 1.4** Typical stress curve of a SMA at a temperature above $A_f$ [5].

The thermodynamic stability of the austenite structure increases at temperature above $A_f$. Therefore, UPS and LPS values ascend with increasing temperature. However, at temperatures above the martensite deformation (Md) value, no superelasticity

is observed since the material will reach yield stress. (Figure 1.5)

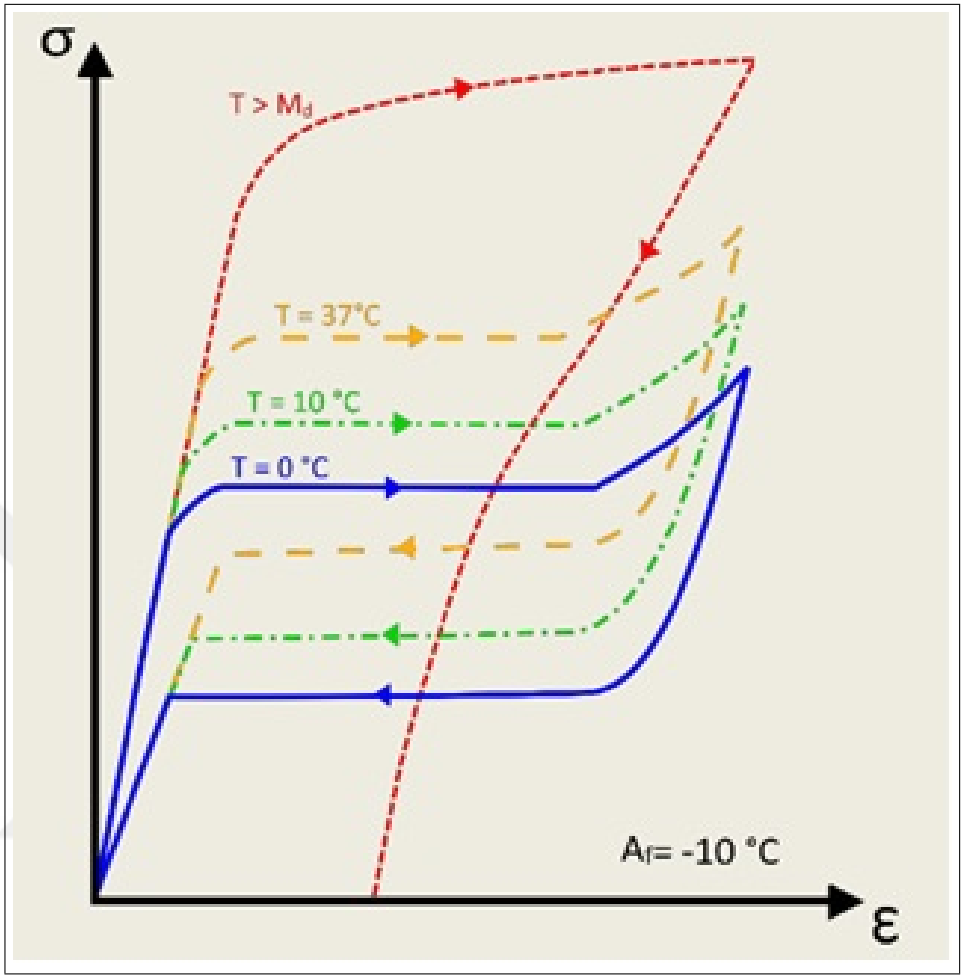


**Figure 1.5** An example of superelasticity behaviour of a SMA at various temperatures [1].

### 1.1.5 Outstanding Features of SMAs

Today, there are memory alloys made of a wide variety of materials, and each one has its own physical and chemical properties. In terms of biomedical applications, NiTis stand out among other SMAs with their superior properties. Some of these properties are high biocompatibility and mechanical strength.

The biocompatibility of NiTi has been studied in many studies due to its high content of Ni element. However, the strong metallic bond between the Ni and Ti elements composing NiTi makes Ni release difficult. In addition, surface treatment

processes, such as forming a protective $TiO_2$ layer [6] or coating with TiN/Ti (Titanium nitride) [7] minimize Ni release. It has been shown in the studies that a NiTi produced according to the standards with protective $TiO_2$ layer is better resistance to corrosion than stainless [8] and causes less Ni release than a human's daily diet. In vitro and in vivo tests have shown that NiTi are highly bio-compatible. Today, SMAs are used safely in many FDA approved commercial products such as vena cava filter (Simon Nitinol, Becton Dickinson, USA), guidewire (Nicore, Bard Medical, USA) and stone retrieval basket (Segura Hemisphere, Boston Scientific, USA).

Nitinols are preferred in many medical products due to their superior mechanical properties as well as being biocompatible. Nitinols are flexible materials and exhibit greater kink resistant compared to stainless steel. They can also successfully transmit the torque applied to them. These characteristics enable the guidewires to perform their movement successfully through tortuous tracts in the vessel, urinary canal and body cavities.

In the process of tooth reshaping, the orthodontic archwires must exert a constant pressure to the teeth. For this reason, the tension of the archwires produced from conventional materials such as stainless steel is readjusted over time. On the other hand, the high strain of NiTi's under load makes them a strong candidate for archwires production.

In addition to the aforementioned properties, the ability to determine of the mechanical characteristics of nitinol in the production stage has led them to become the desired material for medical applications [9].

### 1.1.6 SMAs for Actuator Applications

SMAs have been used in the fabrication of a large number of actuators that serve various purposes. Their shape memory effect with temperature change makes them a powerful candidate in actuator design. SMAs arrive at the target geometric form and

provides actuation at temperatures above the Austenite transformation temperature; however, they need a force to cause deformation in order to perform repeated actuation of SMAs. In the direction of the force called bias force, the SMA returns to its deformed state before stimulation. Various approaches have been developed in order to provide bias force in actuator design. These are gravitation, spring and antagonistic bias mechanisms.

Superior properties of SMAs and especially NiTi's such as high work output with relatively high operation frequency, gradual contractibility, long-term stable and quiet operation make them stand out for actuator applications.

### 1.1.7 SMA Shape Setting

There are some limitations to the use of SMA wires in the actuator mechanism, the largest of which is the limited stroke capability of the wires. Geometric approaches developed to overcome this situation can also benefit to some extent. However, the most efficient solution is to reshape SMAs according to design requirements. At present, SMAs can be formed as an alternative to SMA wires in compression, extension, Belleville disc and cantilever spring or in a different geometric configuration. This makes it possible to implement compact products.

The first step of shaping an SMA is to fix it in the targeted geometry and to heat it for different times depending on the characteristics of the material. These values can range from 350 - 550 °C to 1 - 60 minutes and should be optimized according to the properties of final product [12]. Because higher shaping temperatures and times cause higher actuation temperature of the SMA and sharper thermal response; however, they may reduce maximum output force.

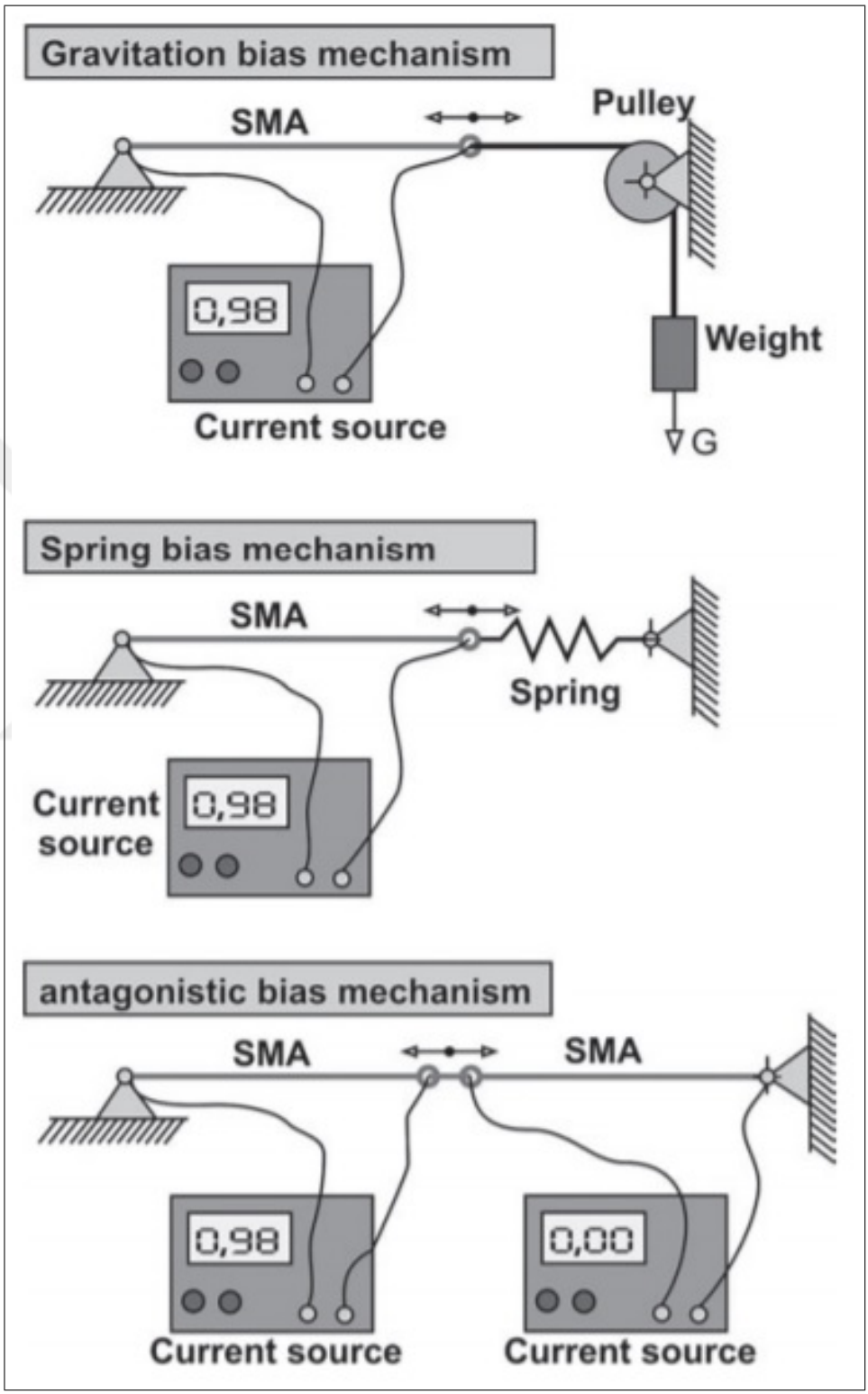


**Figure 1.6** Bias Mechanism Types [10].

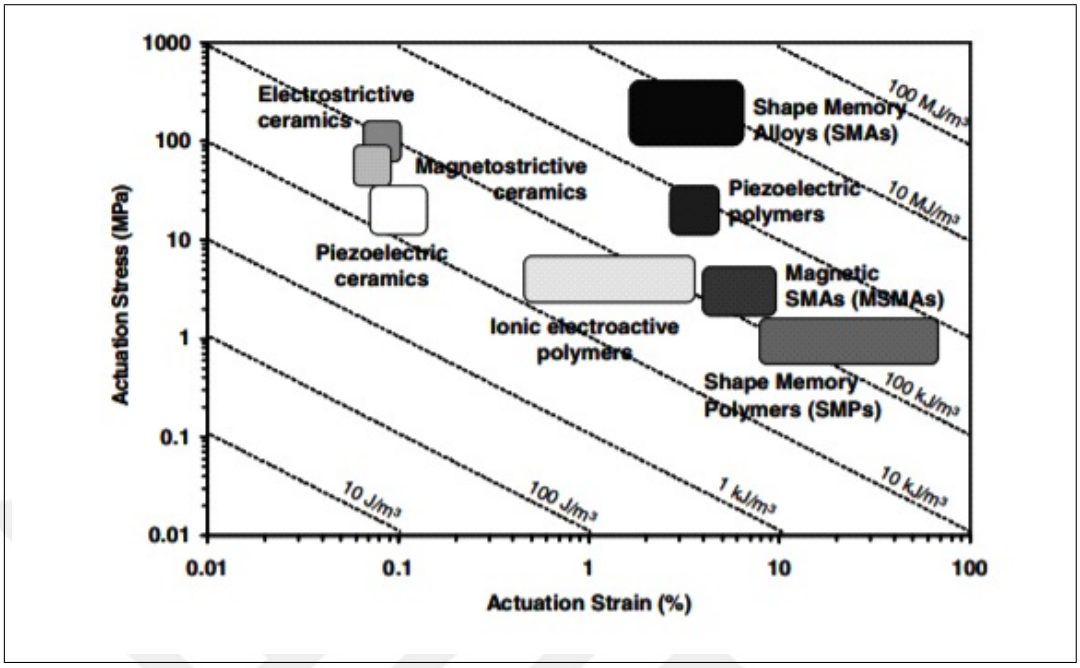


**Figure 1.7** Actuation energy density diagram indicating of various active materials [11].

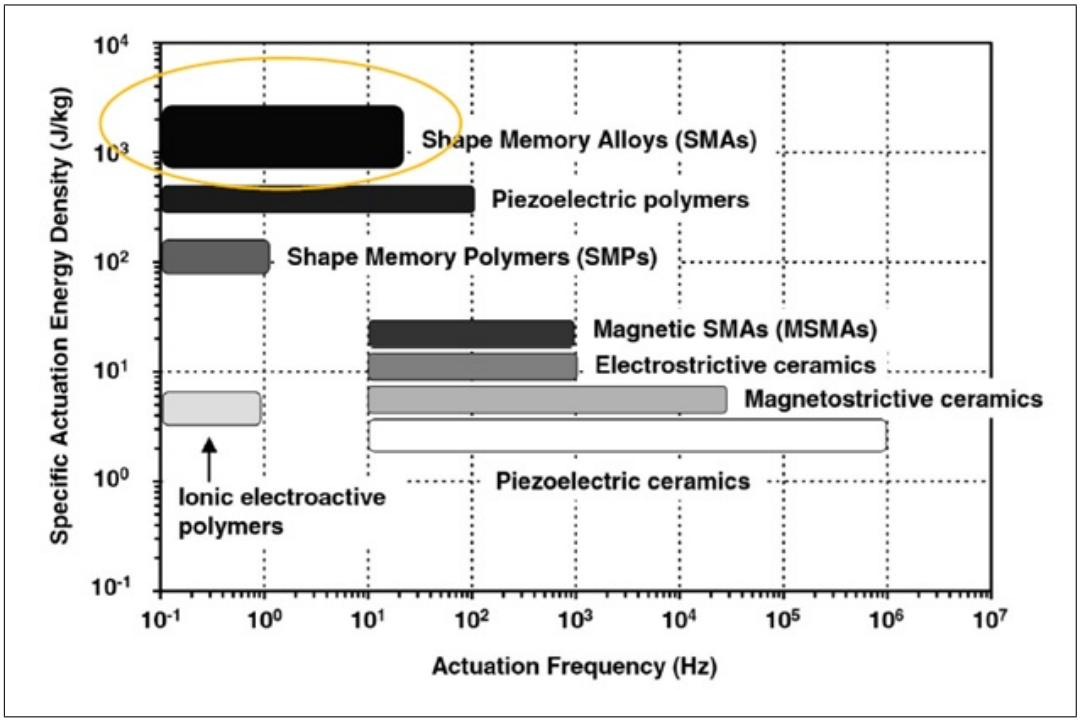


**Figure 1.8** Actuation energy density vs actuation frequency of various active materials [12].

### 1.1.8 Characterization of Transformation Temperatures

**1.1.8.1 Differential Scanning Calorimetry.** Differential Scanning Calorimetry (DSC) is a thermoanalytical technique that shows the alteration of heat capacity of a material at various temperature values. This technique, which examines the required heat flow to change the temperature of a material with a certain mass, is widely used to determine the phase transition temperatures of SMAs [13] . The fluctuation in the endothermic section of the DSC curve indicates austenite transformation temperatures ($A_s$ and $A_f$) of the SMAs, while the exothermic section shows the martensite transformation ($M_s$ and $M_f$) temperatures.

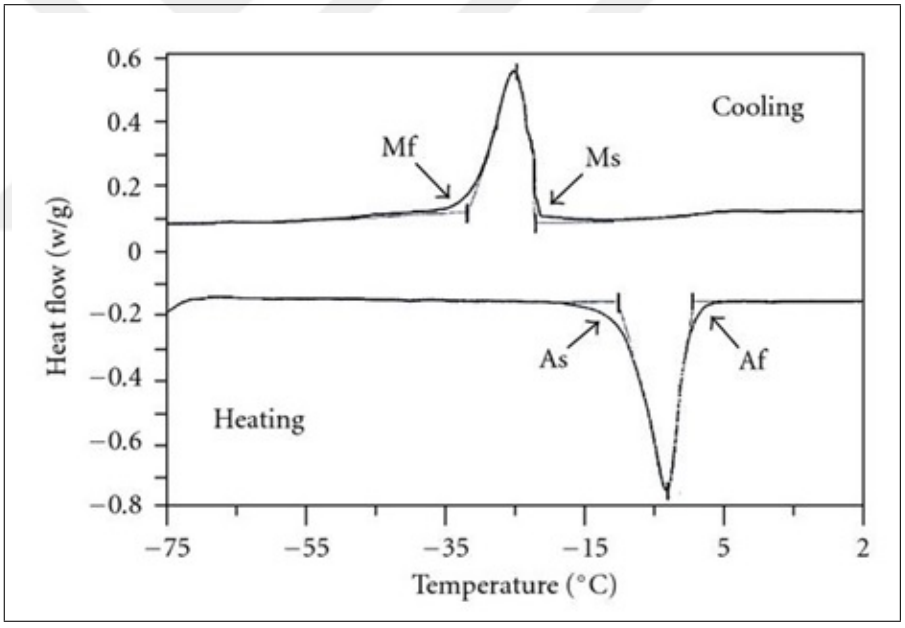


**Figure 1.9** A DSC curve showing phase transformation temperatures of an SMA [14].

**1.1.8.2 Bend and Free Recovery.** Bend and Free Recovery (BFR) is a test method used to determine of martensite to austenite transformation temperatures of SMAs. This test method is based on the principle of deformation of an SMA sample in martensite form and then recovery of structure at certain temperatures. Figure 1.10 shows the macro-scale reflection of the crystal structure change in response to the temperature increase of an SMA in detwinned martensite structure. $A_s$ and $A_f$ tem-

peratures of the sample are determined from this graph using tangent methodology [15].

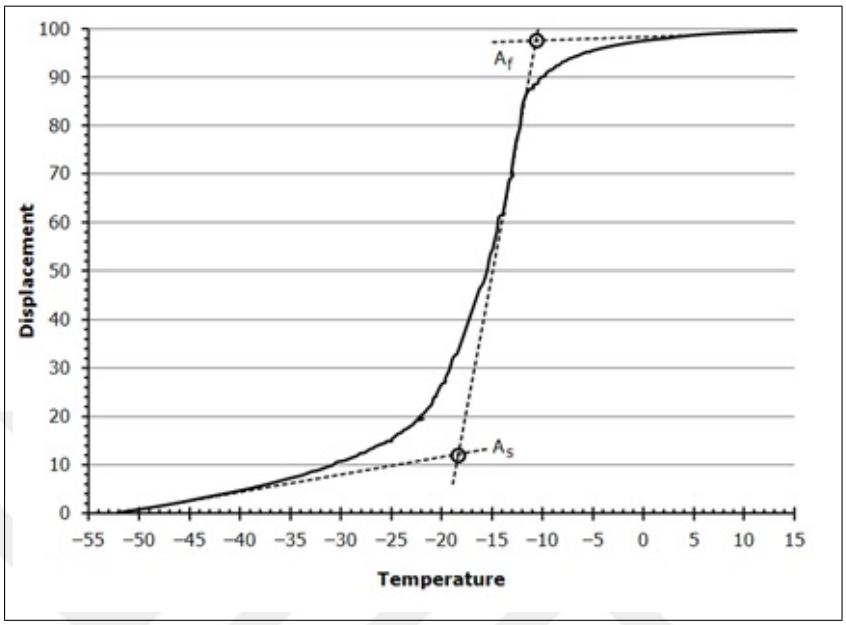


**Figure 1.10** BFR example of an SMA [15].

## 1.2 Tissue Response

Following peripheral nerve electrode (PNE) application to the nerve tissue, a tissue response develops due to the surface chemistry and molecular modification, mechanical and electrical effects of the applied electrode. The mechanical effects that make up the tissue response following the implantation are mostly the changes in the blood flow and the reflections of the tissue-electrode mechanical incompatibilities.

The vessels involved in perfusion of peripheral nerves are highly prone to mechanical effects. The blood flow in the endoneurium varies in the direction of intrafascicular pressure. Only a small decrease in venular flow up to 20 mmHg occurs, while capillary and arterial flow decreases above this value. Venular flow stops at approximately 60 mmHg and whole blood flow stops at 70 mmHg [16]. These pressure values are responsible for nerve damage seen in compression neuropathies.

Changes in pressure value influence axonal transport as well as blood flow. There is no change in axonal transport up to 20 mmHg, but transport level above this value decreases significantly.

Not only the pressure increase, but also the strain on the nerve influences the blood flow. Arteriolar and capillary flow starts to be affected at 8% strain and at 10% strain, and when 15% strain is reached, blood flow is completely stopped [17].

Pressure-related changes in the peripheral nerves vary with the pressure value and duration of the nerve. Short-term acute compressions, nerve ischemia, hypoxia, edema, vascular permeability and axoplasmic flow leads to a decrease while long-term compressions affect microcirculation. Decrease in microcirculation causes distal and axonal disintegration and degeneration of myelin sheets and loose of motor function [18].

Neural tissues have a soft structure with viscoelastic and elastic modulus ranging from 100 to 1000 Pa [19]. Many studies on cell biomechanics have proven to be highly susceptible to mechanical changes around cells [20].

Biomechanical and structural mismatches between an applied electrode and tissue cause the stimulation of the foreign body reaction mechanism [21]. This mechanism results in inflammation and wound formation. As the fibrous tissue covers the active regions of the electrode, the tissue-electrode interface impedance value increases, which makes it impossible for the electrode to operate stable for a long time. Moreover, a chronic friction motion causing wear on the tissue also causes structural deterioration.

Different approaches have been developed to eliminate mechanical discrepancies between neural tissue and electrode. One of these approaches is the selection of materials with low elastic moduli in electrode production. Electrodes produced from substrates such as Polyimide (8.45 GPa) [22],[23], Parylene C (4 GPa) [24], [25] and PDMS (1 MPa) [26] with various elastic modules have been proven to cause less neural tissue damage compared to rigid material.

Composite FINEs with patterned stiffness have been developed to reduce tissue response in FINE electrodes aiming to achieve an oblong geometric structure of nerve tissue. These electrodes are produced by placing the rigid material between the soft material such as silicone to shape the nerve to the targeted geometry. Preliminary studies show that C-FINE design does not cause any change in axonal morphology (axon density and g-ratio) and electrophysiology and does not cause neuropathy [27].

Another method developed to eliminate neural tissue discomfort is to change the electrode geometry. PI Nanofiber based nerve electrodes have minimized mechanical incompatibility due to their porous structure and also did not prevent nutrient and oxygen transmission. It has also been shown that modification of the electrode surface with anti-inflammatory drugs reduces foreign tissue response [28].

# 2. MATERIALS and METHODS

## 2.1 SMA Spring Shaping

The implant electrodes should be as compact as possible. For this reason, the actuation mechanism that will provide the clamping movement must also meet this requirement. Therefore, SMA wires (Flexinol, 150 $\mu m$ Diameter) are shaped as springs in order to provide high movement in limited dimensions. The wires were wound around the metric 1.6 bolt at 129 g constant load and fixed. Then it was annealed at 520 °C for 12 minutes and immediately quenched in water at room temperature. The fabricated SMA springs were placed in the test apparatus created by us in order to make characterizations. The SMA spring in the form of twinned martensite was fixed at one end to the forcemeter and at the other end to the mobile platform. The effects of different DC current applications at different strain levels on force generation as well as spring heating and cooling profiles were examined.

## 2.2 Design of Test Platform

The experimental setup to be used in the characterization of the sample was designed by using CAD (Solidworks Corp.) program and realized with the help of 3D printer (Zortrax M200). The digital forcemeter (PCE Instrument-LFG 20) was placed on the platform. Connection points were prepared for placing the NiTi sample on the stage which was positioned against the forcemeter and moving with the screw step.

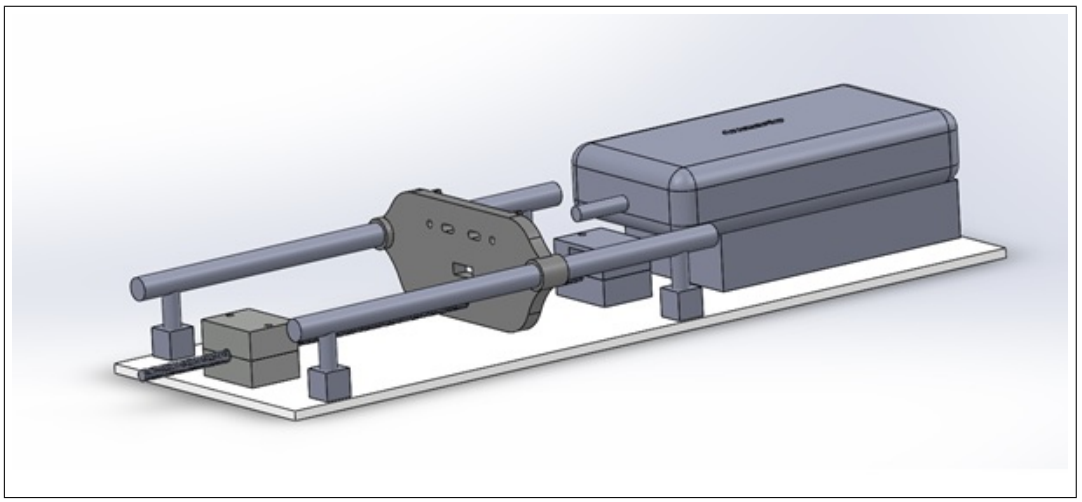

**Figure 2.1** The CAD design of the test setup.

## 2.3 Actuator Frame Design

The FINE frame was designed and built with a 3D printer (Objet 260 Connex) and as shown in Fig. 1, SMA spring was placed in this frame. The linear displacement provided by thermo-mechanic effect of SMA is transferred to the part where the electrode will compress the nerve via an insulating wire.

The pre-manufactured SMA spring was then placed in parallel and physically connected to the electrical contacts by crimper. In order to strengthen the bond, Dymax 203A-CTH-F and 204-CTH-F (Dynalloy) adhesives were applied with 1: 1 mixing and cured with UV.

The bias force required for SMA to perform repetitive contraction-relaxation movement was provided with superelastic NiTi wire (500x100$\mu$m). During the 3D fabrication, two superelastic nitinol were embedded in the 3D structure parallel to each other. It was then fixed to the main frame with a UV adhesive.

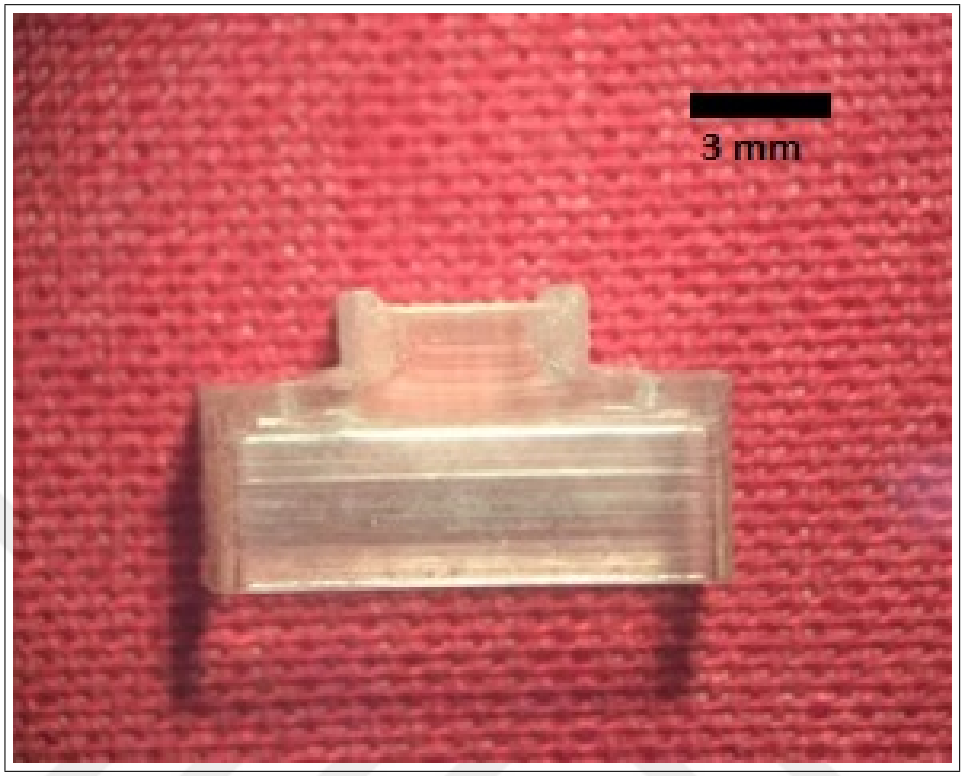


**Figure 2.2** The FINE main frame.

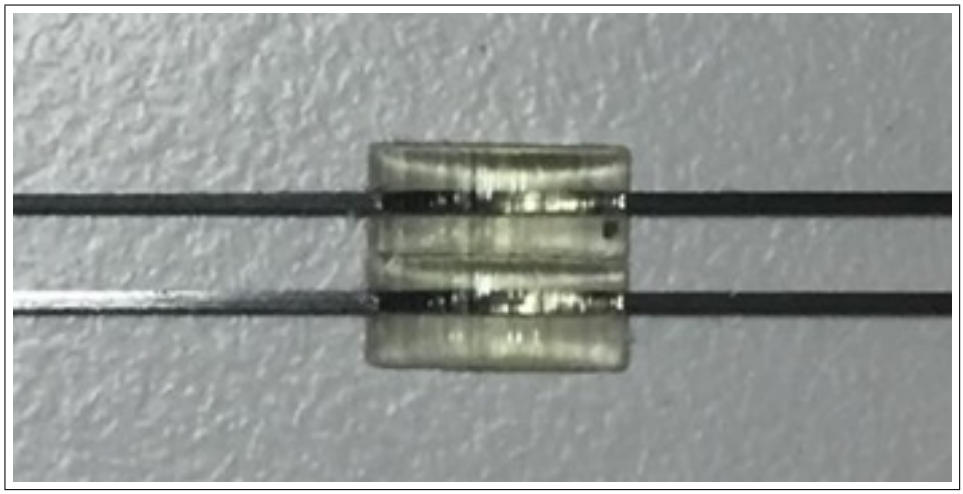

**Figure 2.3** Bias force part.

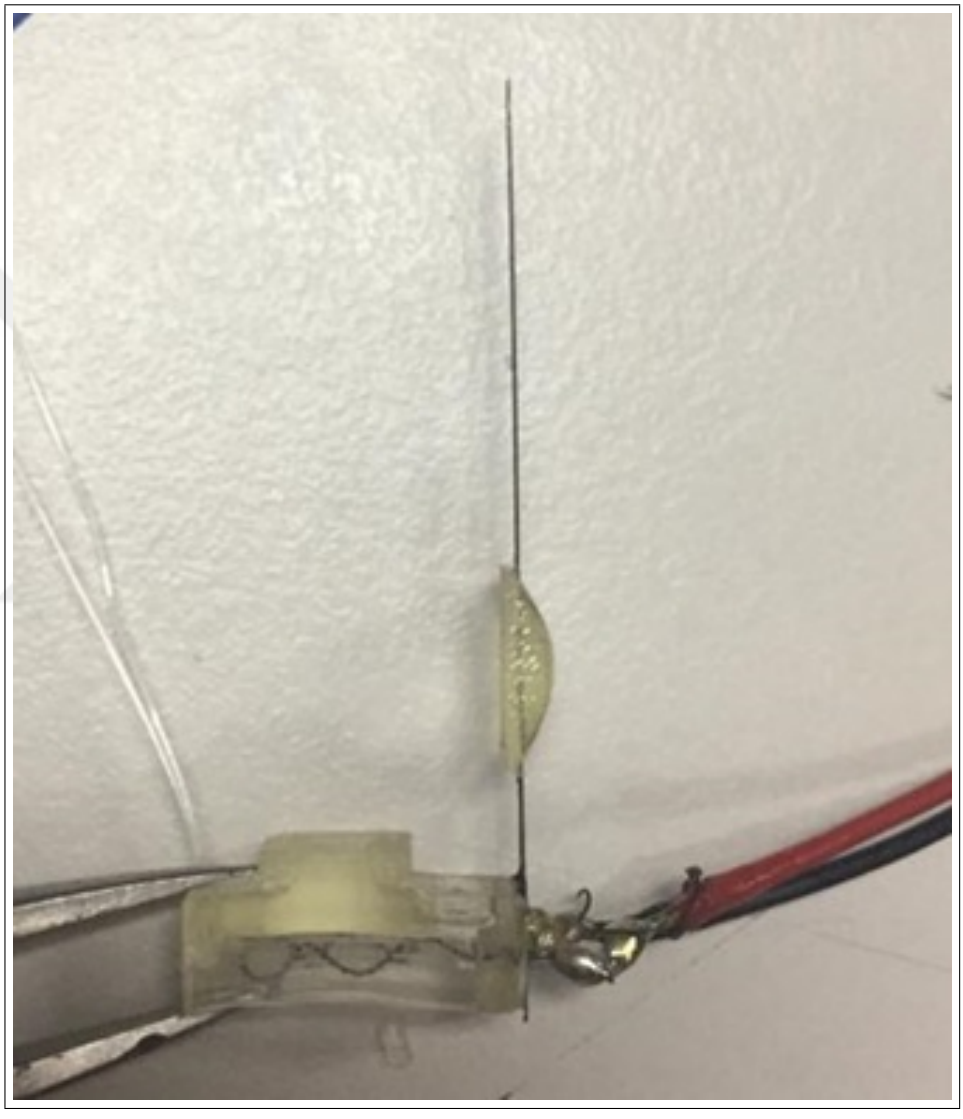

**Figure 2.4** The NiTi based prototype.

## 2.4 Actuation Control Unit

Since the heating of nitinol spring will be provided by electric current, the architecture shown in the diagram below was designed for the control of the contraction mechanism.

The control mechanism consists of 4 main components; LabVIEW program, Arduino Mega, voltage and current sensor unit (INA260), and a mosfet (IRL540N).

The Labview program enables the simultaneous electrical stimulation and data acquisition over the computer and allows easy determination of the test parameters.

With the $I^2C$ communication protocol, the Arduino collects data from the voltage and current sensor unit, and also triggers mosfet with the digital pin. In addition, the voltage and current sensor unit and other electronic components were placed on the PCB to form an Arduino Mega compatible module.

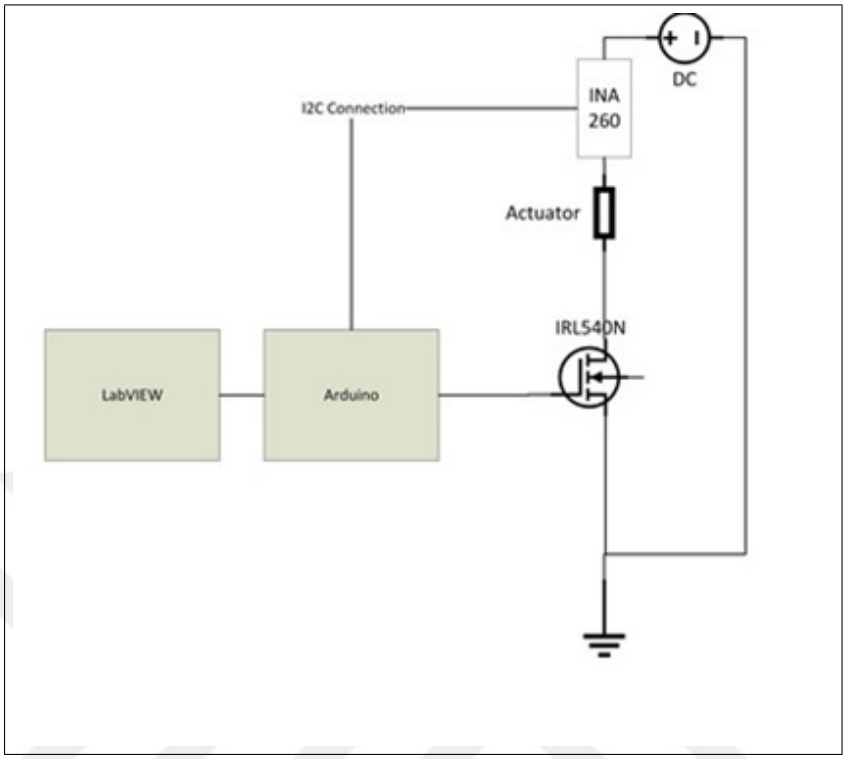


**Figure 2.5** NiTi based actuator control schematics.

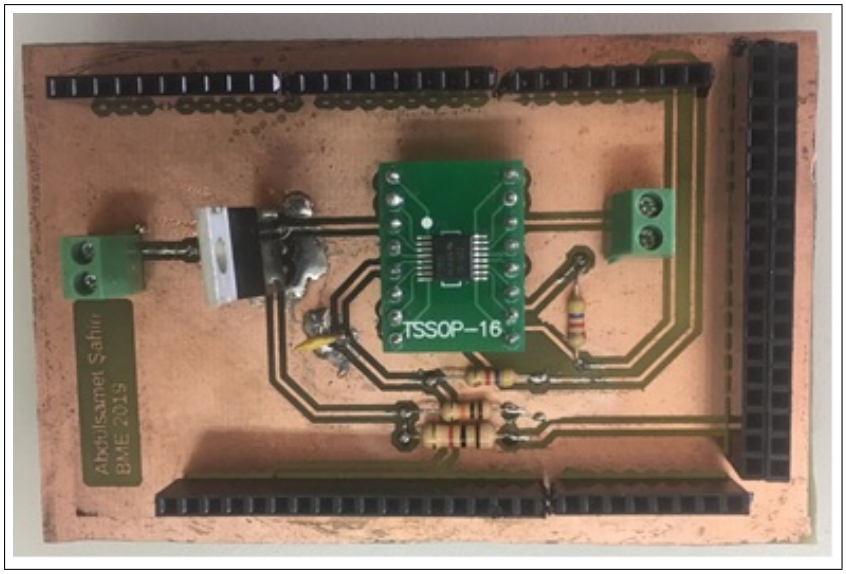


**Figure 2.6** Arduino Mega compatible module.

## 2.5 Characterization of the Actuator

The bias force, which enables repetitive movement, must be large enough to convert the NiTi spring back into detwinned martensite form after contraction In order to determine the force generated by the bias mechanism provided with superelastic nitinols, the actuator was placed on the force measuring platform as shown in the photo, mimicking the contraction mechanism.

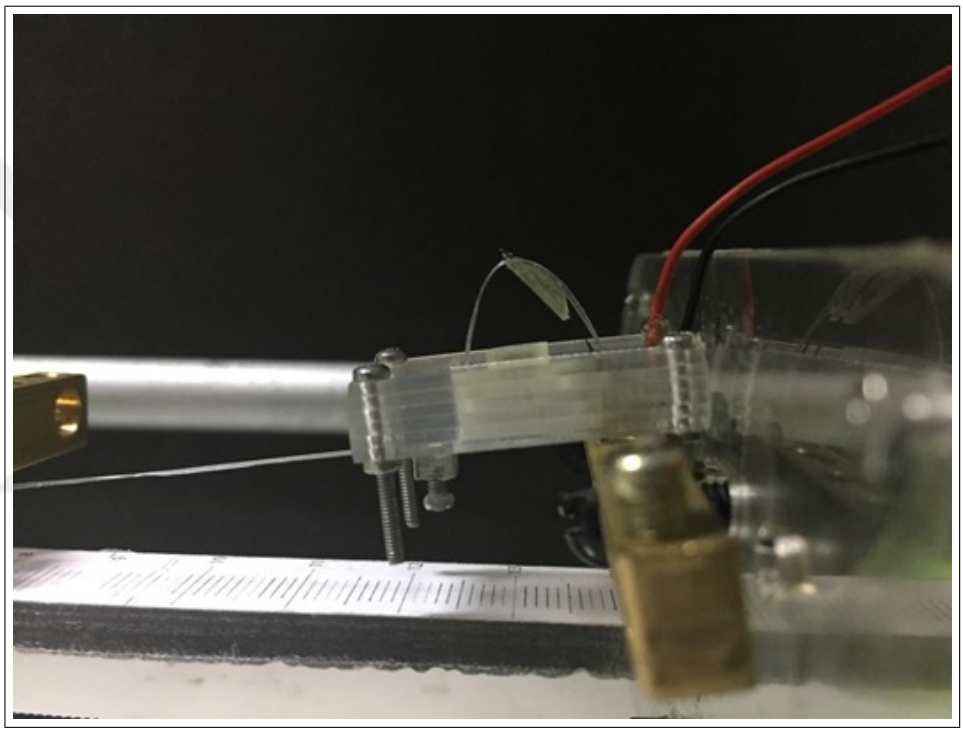

**Figure 2.7** The test setup for measuring bias force.

## 2.6 Electrode Design

Polyimide (PI) is a flexible material with high mechanical and chemical resistance and is therefore widely used in flexible sensor and electrode applications. Because of these superior properties, an electrode was constructed on PI sheet in this study. PI, whose surface was cleaned with acetone and isopropyl alcohol, was fixed onto a silicon wafer. The paper tape was glued to cover the PI. The CAD design shown in Figure 2.8 was processed on PI with a $CO_2$ laser (Epilog Engraver). Laser power was used at

a level that could only cut paper tape, as determined in the preliminary studies. The cut parts were mechanically cleaned from the surface. PI with a stencil on the surface was placed in the PVD device. The surface was coated with 30 nm chromium and 150 nm gold, respectively. The template was mechanically cleaned from the surface. The electrode was examined under a microscope and short-circuit control was performed. As a result of the measurement, the resistance of the paths was evaluated.

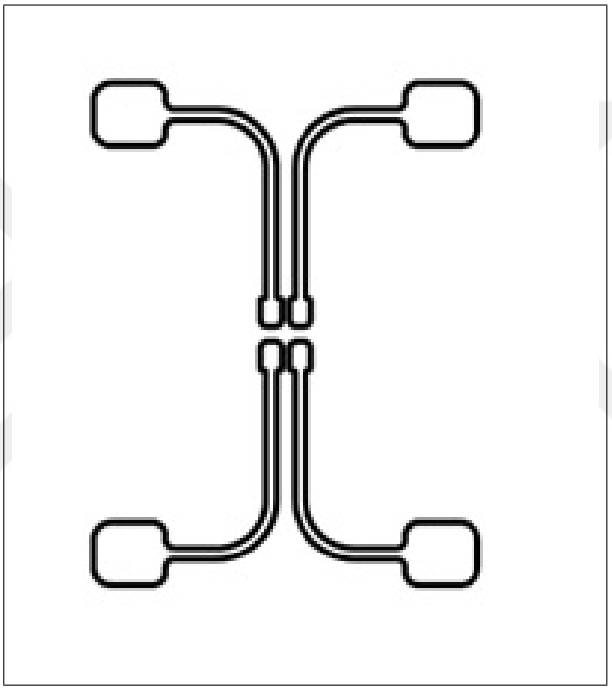

**Figure 2.8** The CAD design of electrode contacts.

## 2.7 Sciatic Nerve Test

The designed actuator mechanism was tested on two sciatic nerves obtained from a water frog (Rana Ridibunda). The frog was double pithed prior to dissection. The experiment was approved by the Institutional Ethics Committee for Animal Experiments and Care of Bogazici University. The compression success of the actuator was tested by the following test apparatus. The actuator was placed between the stimulating and recording electrodes and the effect of the degree of compression on compound action potential (CAP) was examined. Stimulation of the nerves was per-

formed with the signal generated by the custom-made signal generator. The stimulus was a current pulse with amplitude 0.2 mA and duration 0.25 ms. In addition, isolation of the stimulus signal was achieved with an analog signal isolator (Model 2200, A-M Systems). CAP values were amplified by 100 times with custom-made amplifier. The stimulation signal (Channel 1) and the resulting signal (Channel 2) were examined with a digital oscilloscope (ADS-3072B, AA Tech). The effect of the pressure created on the nerve by driving (by 350 mA) of the designed actuation mechanism on signal conduction through the nerve was evaluated by CAP values.

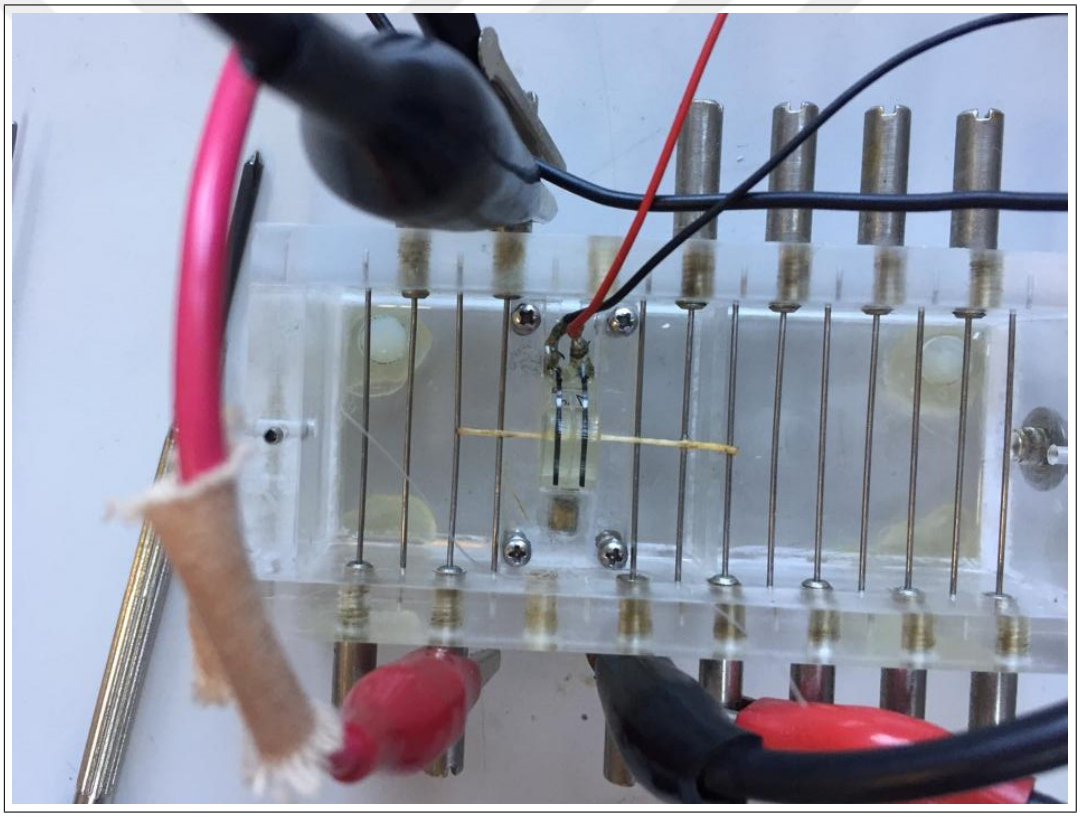

**Figure 2.9** CAP measurement setup.

# 3. RESULTS

Figure 3.1 shows the sections of the SMA spring forming process to be used in the actuation mechanism. Section 3.1a shows the SMA spring in the form of detwinned martensite after forming the section 3.1 b of the SMA wire wound on the metric 1.6 bolt and fixed under constant load.

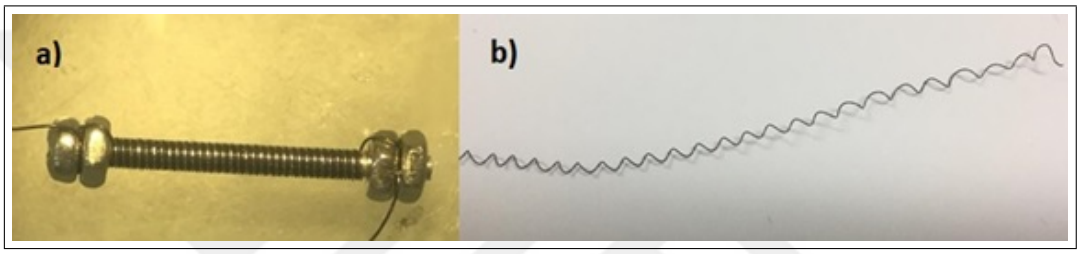


**Figure 3.1** Preparation of the wires for the shape setting process (a). Final form of the spring after heat treatment (b).

The test platform prepared by assembling the parts manufactured according to the CAD design and placing the forcemeter is shown in figure 3.2. There are two points on this platform to which SMA broadcast connects. One of these points is connected to the force meter while the other moves on the rails and thus makes it possible to take measurements of different lengths. The movable platform moves back and forth with the rotation of the metric 6 shaft. This ensures precise pitch between turns. The displacement can be determined by the screw step as well as by means of the center ruler. In addition, the spring can be easily integrated into the platform with a screw and is not affected by mechanical stress from electrical contacts.

The results of our experiment to find the maximum force values generated by SMA spring at different strain values are shown in Figures 3.3 and 3.4. Table 3.1 shows the amount of pulling corresponding to the groups. In Figure 3.3, the excitation was performed with lower electric current amplitude. The reason for this is to prevent overheating of the SMA spring and the deterioration of its structure as plastic. However,

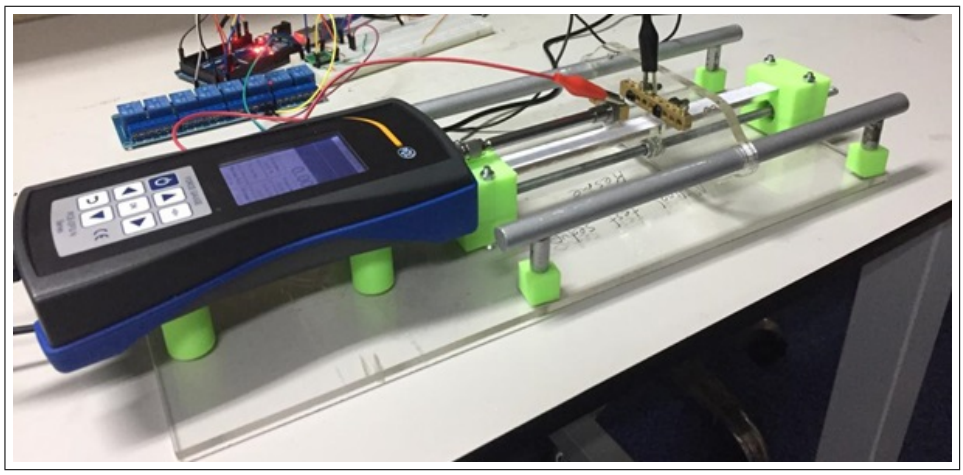

**Figure 3.2** NiTi spring characterization setup.

**Table 3.1**
Elongation amounts of the SMA springs extended in various quantities.

| Group Number | Group Displacement (mm) |
|---|---|
| 1 | 0 |
| 2 | 7 |
| 3 | 12 |
| 4 | 17 |
| 5 | 22 |
| 6 | 27 |
| 7 | 37 |
| 8 | 52 |
| 9 | 67 |

in all graphs, increasing current values and rising force values are noteworthy.

Figure 3.5 shows the forces generated by the excitation of springs drawn at different lengths with 320 mA. It is evident that the increased amount of tension increases the force generated by the spring despite the excitation by constant current.

Figure 3.6 shows the effect of different current applications on force on group

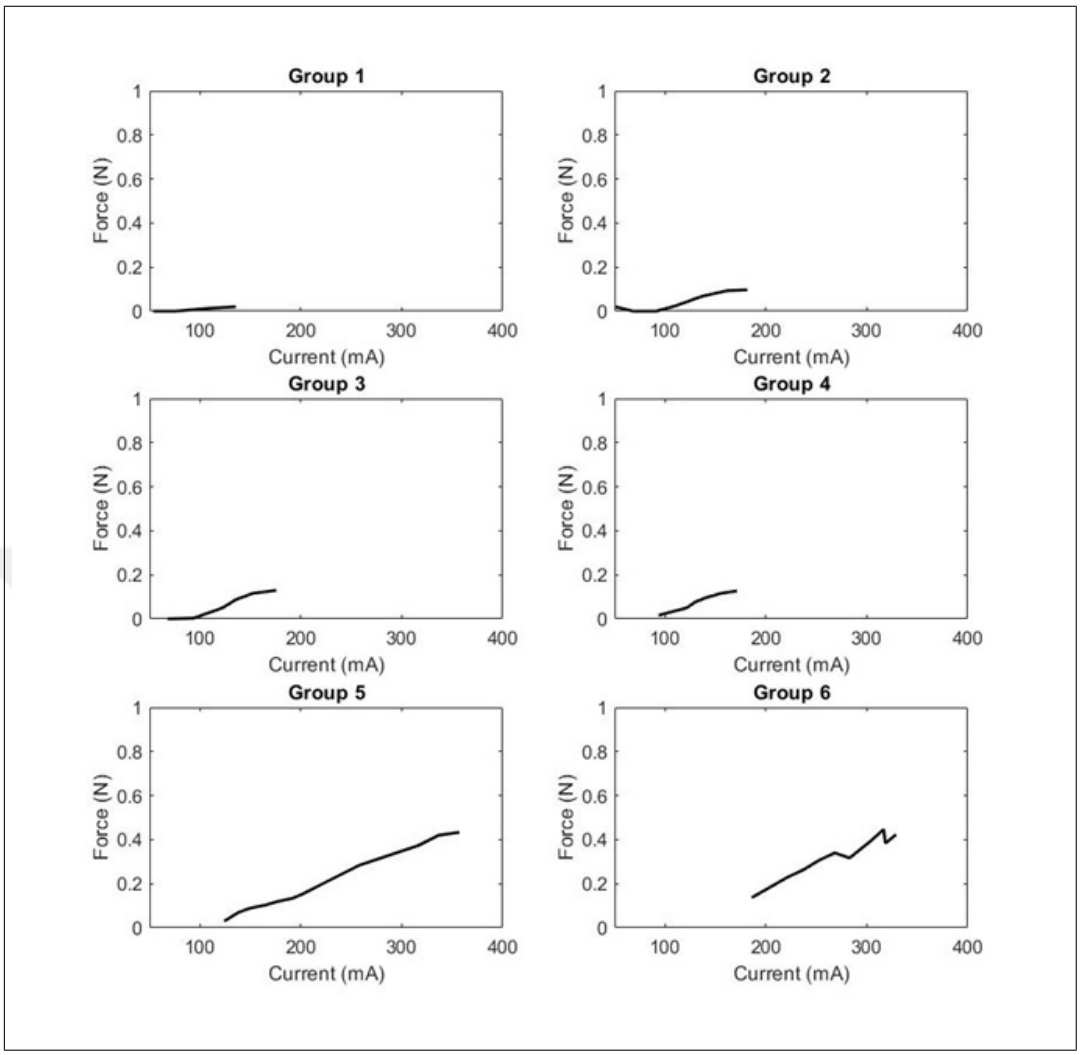


**Figure 3.3** Generated block force with different actuation electrical currents for various lengths of stretched spring .

9 drawn 67 mm. At low current values, no change in the amount of force generated is observed, but with increasing current, the force generated increases rapidly. After a certain period of time in all current values, the force has reached a constant form. In addition, due to high current values causing overheating, low stimulation was performed. As the excitation ends, the cooling profile of the spring can also be seen in the graph.

Figure 3.7 shows the excitation profile of group 9 with 370 mA. The sample quickly reached its maximum force value under high current value and reached equilibrium there. The cooling that occurs with the end of the excitation is shown in the

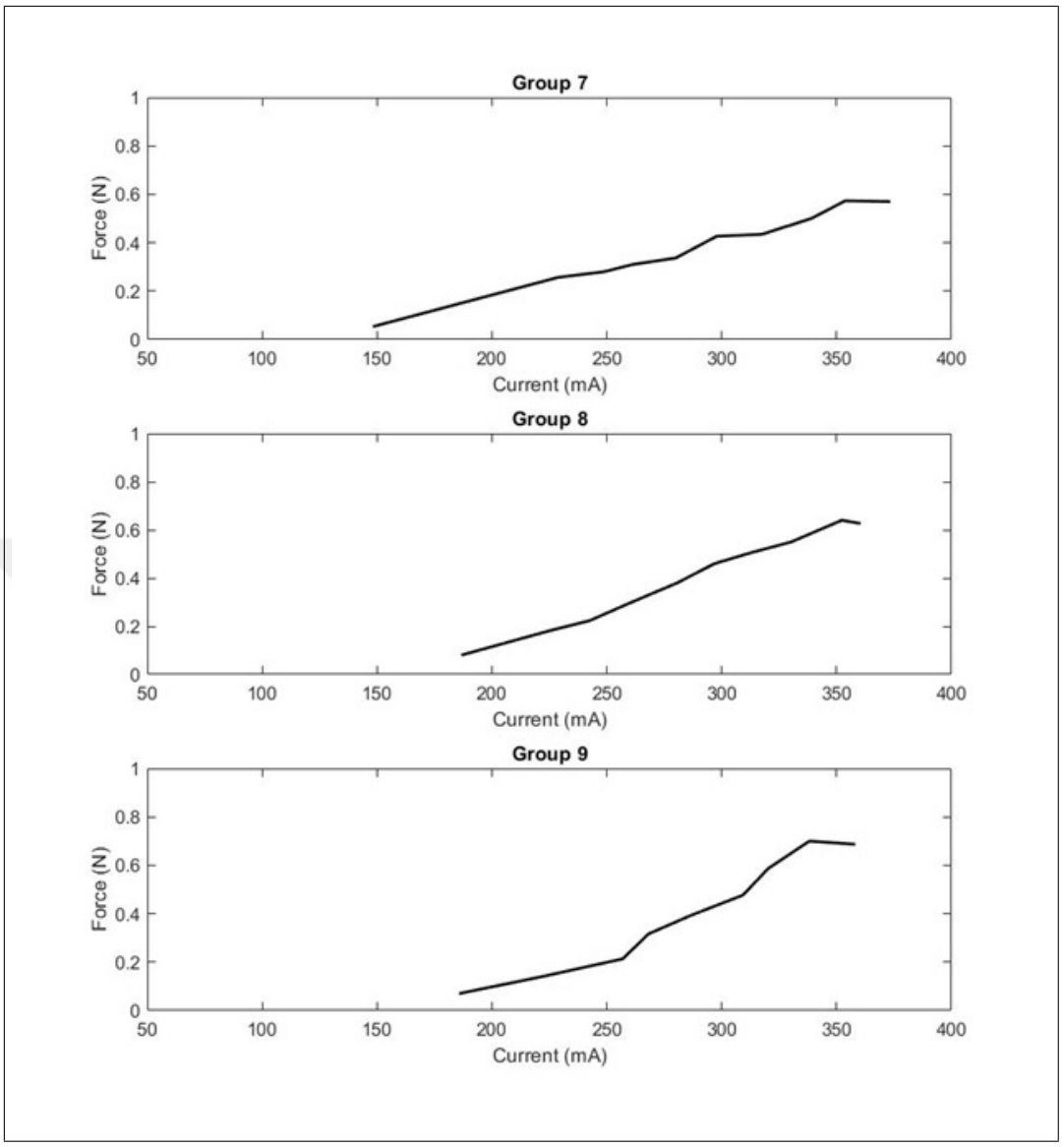


**Figure 3.4** Generated block force with different actuation electrical currents for various lengths of stretched spring.

graph.

The change in current and resistance over time of 4V applied sample is seen in figure 3.8. A sudden decrease in excitation was observed with an increase in resistance value over time and then equilibrium. Figure 3.8 shows the change in resistance caused by the electrical stimulation of the SMA spring and the force values generated by the spring, simultaneously. The sample was stimulated with 4V voltage for 7 seconds. In the first phase of stimulation, there is a sudden drop in resistance. However, an

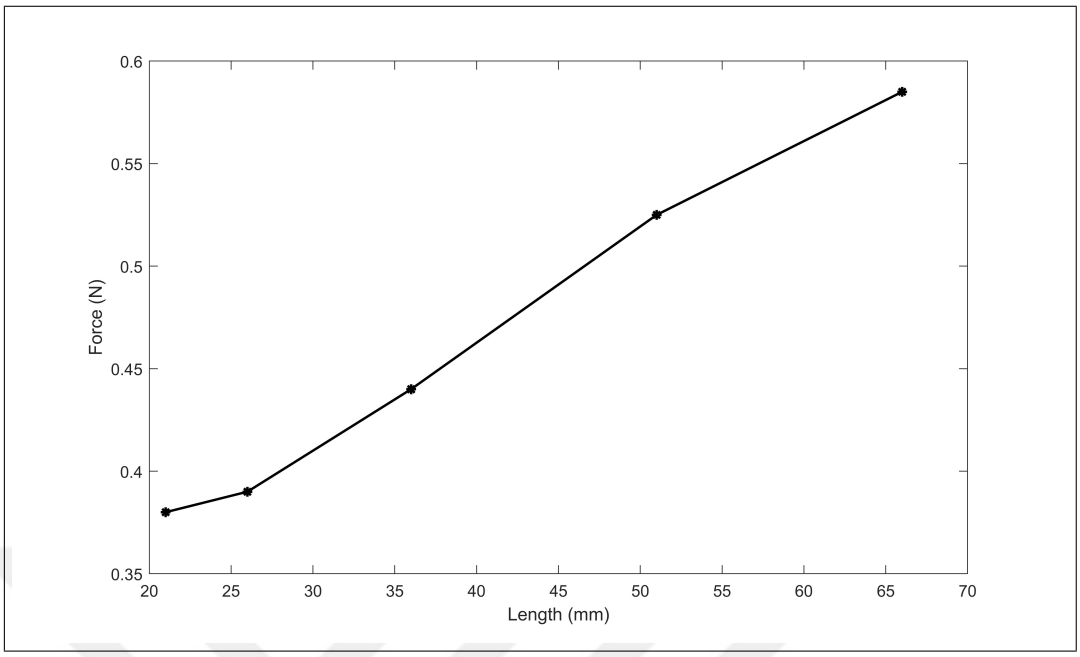


**Figure 3.5** Actuation force of the spring at different stretching length with constant current (320mA).

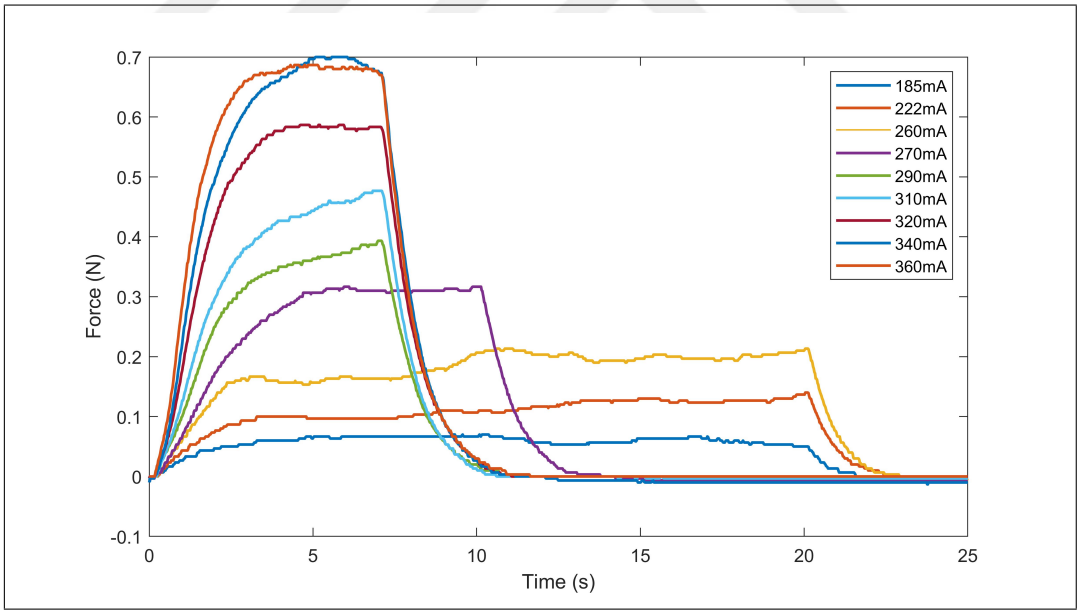


**Figure 3.6** Generated force profile against time produced with different electrical currents.

increase in resistance value over time and then equilibrium was observed. At the end of the electrical stimulation, the resistance value was lost, simultaneously. But the force change was observed for a while.

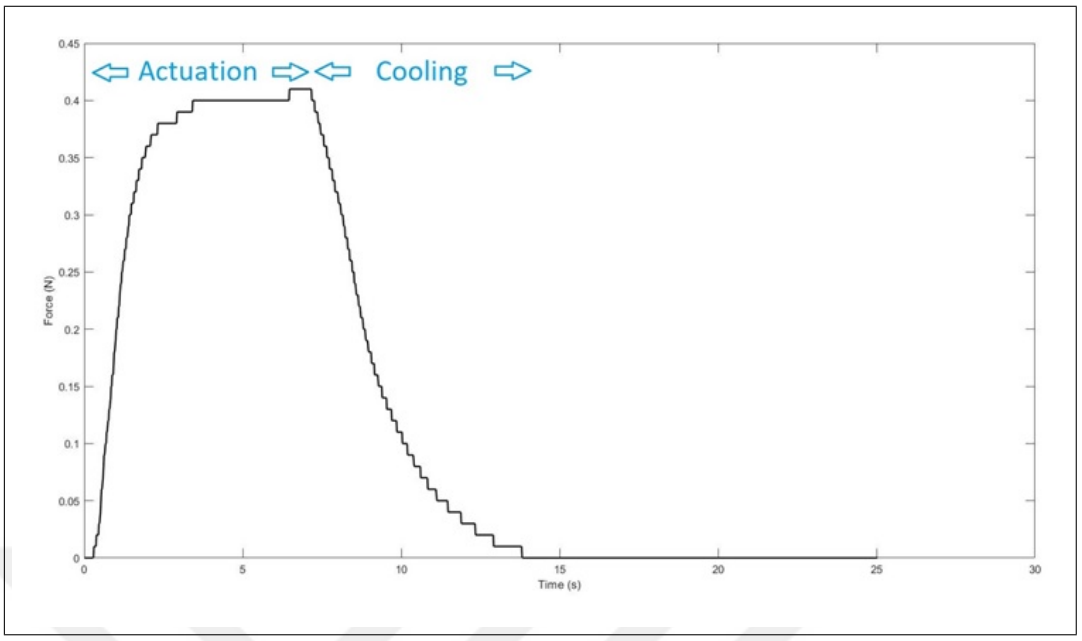


**Figure 3.7** Force profile of the spring actuated with 370 mA.

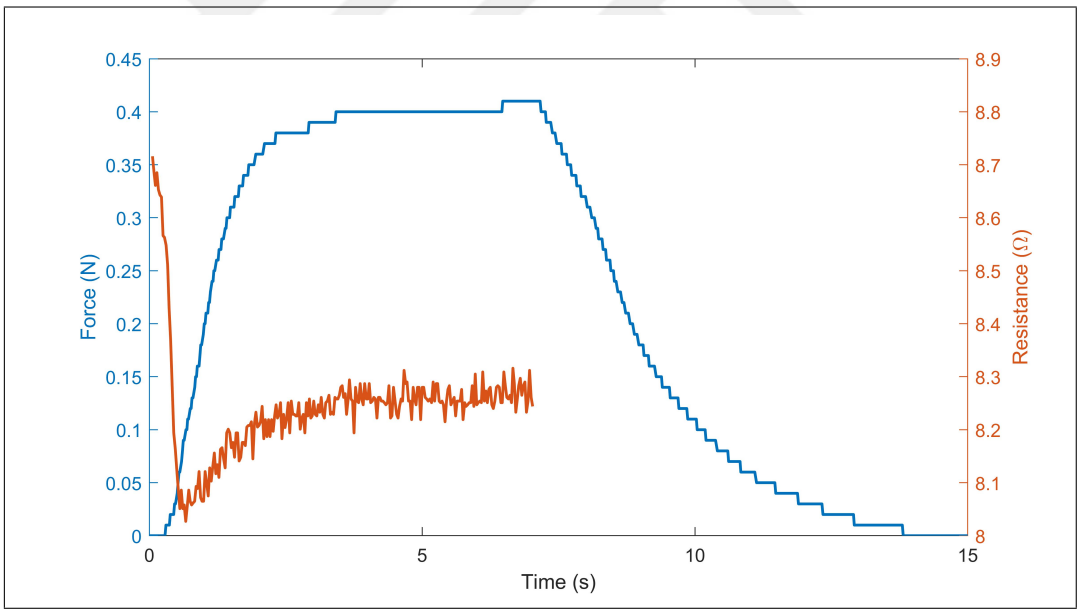


**Figure 3.8** Force and electrical resistance profile against time.

The bias force profile of the manufactured actuator is shown in figure 3.9. While increasing linearly with increasing traction, multiple high force requirements are encountered with tensile quantities over 11 mm.

Figure 3.10 Actuator status at different tensile levels during bias force measure-

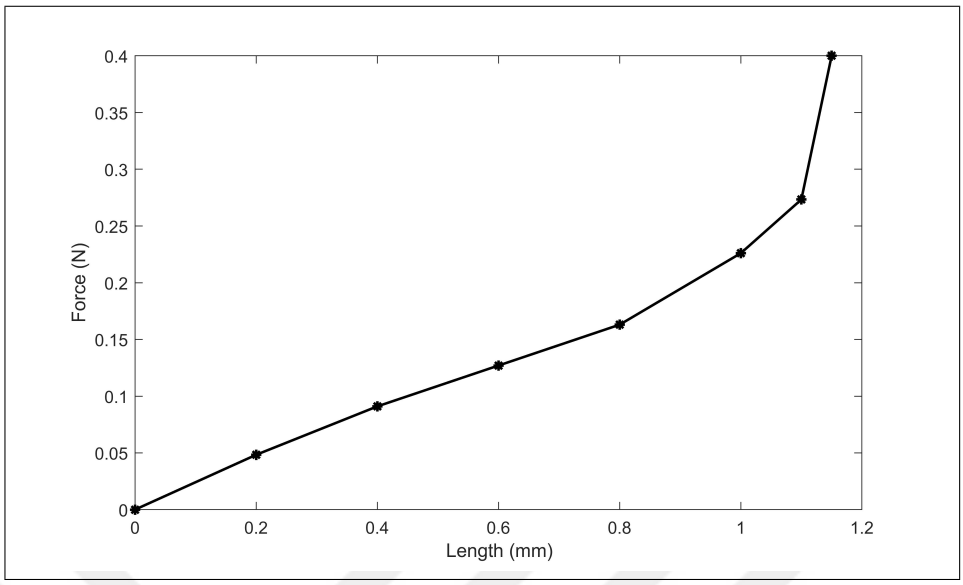


**Figure 3.9** Bias force profile.

ment, 2, 6, 10 and 11 mm, respectively.

Figure 3.11 shows the electrode images resulting from the cleaning of the template after coating with the PVD technique. As a result of the examination, it was found that there was no short circuit between the paths and each path showed resistance up to 11 ohms.

Figure 3.12 shows the stimulation signal of the nerve (Channel 1) and the CAP value (Channel 2) at a different region of the stimulated nerve when no pressure is exerted on the nerve. As a result of driving the produced compression mechanism (FINE) with 350 mA, the effect of the pressure applied on the nerve on the CAP value is shown in Figure 3.13. Considering these two figures, it is seen that the pressure applied on the nerve weakens the CAP signal.

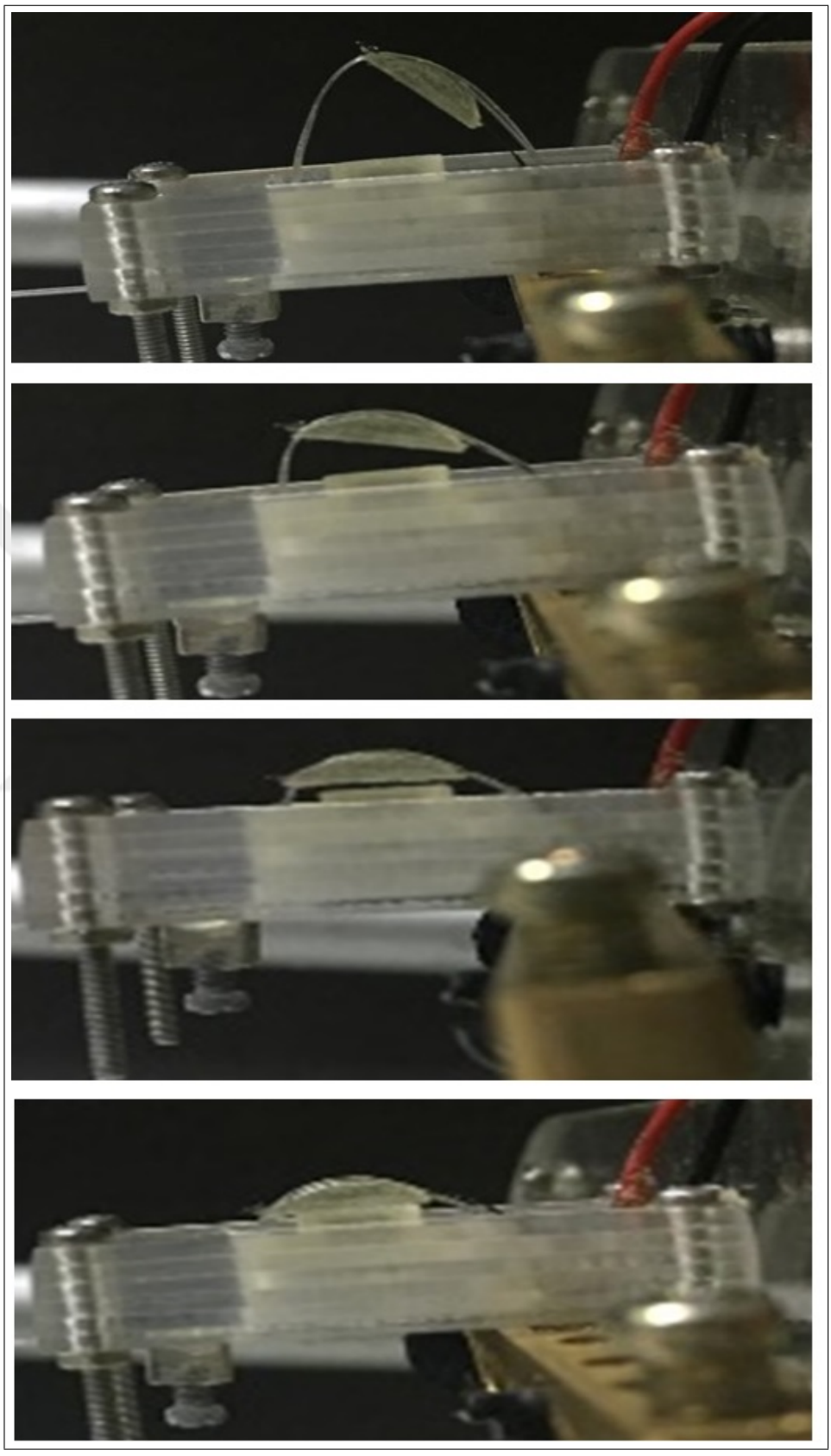

**Figure 3.10** The actuator deformation process during the bias force measurement.

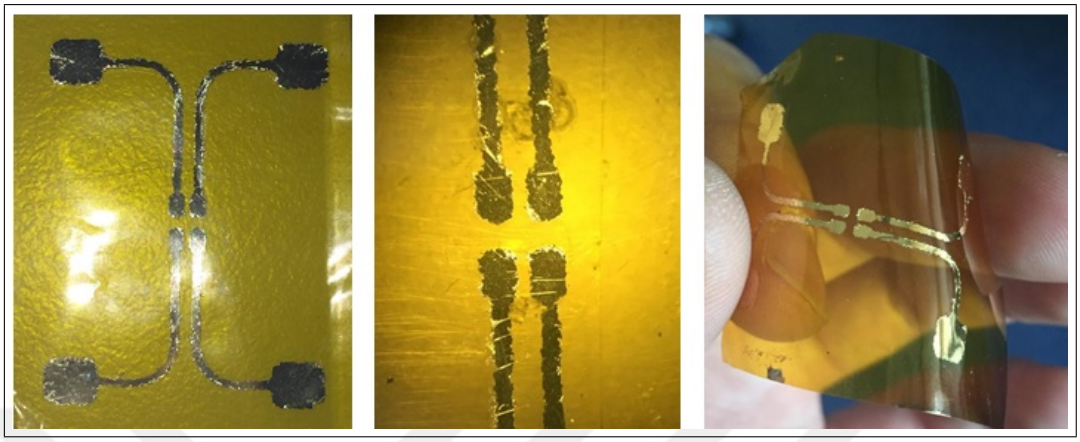

**Figure 3.11** The fabricated electrode on PI sheet using PVD technique.

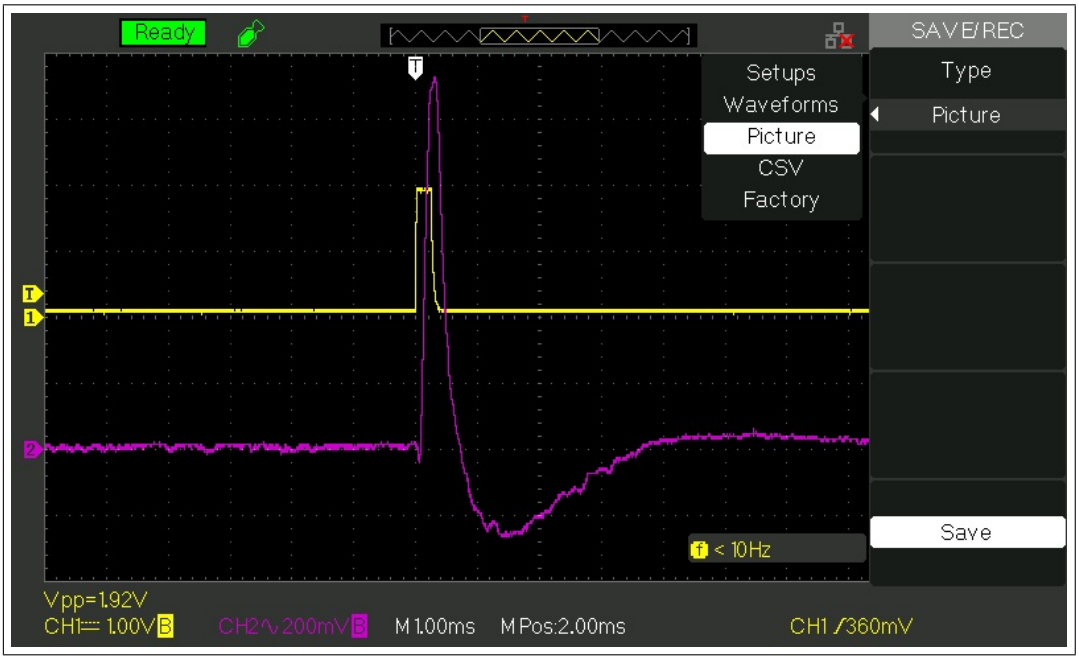


**Figure 3.12** Stimulation signal (Channel 1, current pulse with 0.2 mA and 0.25 ms) and related CAP value (Channel 2, amplified 100 times) before compression of the nerve.

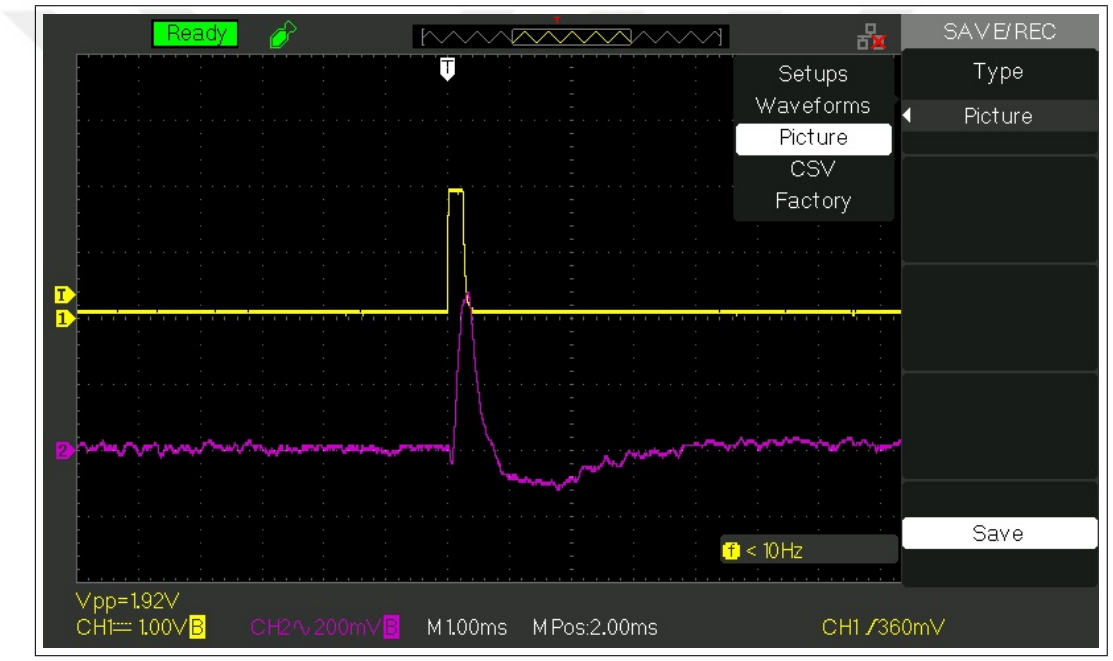


**Figure 3.13** Stimulation signal (Channel 1, current pulse with 0.2 mA and 0.25 ms) and related CAP value (Channel 2, amplified 100 times) during compression of the nerve.

# 4. DISCUSSION

SMAs have been used successfully in many actuator fabrications so far. The fact that they can be individually designed for each actuator mechanism makes them even more valuable. They owe these features to their ability to be reshaped. Nitinol wires, which do not exhibit a high displacement, are reshaped to provide adequate displacement even when used in sizes to be implanted into the body. In this way, the displacement capacity has quadrupled. However, this is accompanied by a severe drop in force. There are several ways to increase the force to be obtained. These are to use thicker wires or to connect multiple wires in parallel. Since the resistance on the thick wires is lower, the amount of current required to heat up is higher, and they will also cool down later, which will reduce the contraction-relaxation frequency. Furthermore, an actuator operating with high current values will cause noise in the electrode part of the system. In this study, the force was increased by using 2 parallel SMA springs in the actuator mechanism in order to avoid being affected by such negativities. The springs were placed in the frame seen in Figure 2.2 and isolated both externally and electrically. The pulling force produced by spring was transmitted to the mechanism to compress the nerve with an insulating wire.

The bias force mechanism in Figure 2.3 was produced because the spring one way we manufactured would work. The amount of force produced by the contraction of superelastic nitinols placed parallel to each other is shown in Figure 3.9. The force generated by SMA spring is far above that. In this way, when austenite form of contraction can be realized and when it cools back to its original state with bias force. This will allow us to make repeated movements. This mechanism worked stably about 300 times during the tests. The recent rise in the graph is due to the attempt to tighten the completely closed mechanism. This is also seen in Figure 3.10.

Figures 3.3 and 3.4 show an increase in the amount of force generated with increasing current values. This can be explained by the fact that the high current

passing spring becomes more heated and can contract even under stress. In order to protect the system from overheating in Figure 3.3, excitation was performed with very low current values and therefore no significant force could be reached compared to the excitations in Figure 3.4.

Figure 3.5 shows the force values produced by the spring drawn at different lengths under 350 mA. Increased traction caused an increase in strength. This may be due to the fact that the crystalline structure approaching the form of detwinned martensite as a result of pulling produces more force.

Figure 3.6 clearly shows the reflection of the current applied to an SMA spring to the force. At high current values, the SMA heats up quickly and produces high forces. It also took a relatively long time to cool down. This is a parameter that should be considered for applications where designs have high contraction relaxation frequencies. The lack of difference in the value of the power produced between 340 and 360 mA can be interpreted as SMA has reached a temperature that will completely transform into austenite form. When the Figure 3.8 is examined, we can say that the resistance value increases with force, that is, with temperature and then comes to equilibrium together.

The process of laser mask formation using paper tape has been very successful in electrode production. Even the closest distance between electrical contacts, 0.4 mm, has been successfully established in this technique. In this way, flexible electrodes can be produced easily and without photolithography.

In the section where the effect of pressure applied on nerve to CAP was examined, various amounts of compression were performed by different DC amplitudes. However, no change in CAP was observed at each compression grade. It is thought that the noise caused by the supply voltage in the system suppresses the change. Only the change observed in Figure 3.13 was noticed at the current value that provides very high compression. Figures 3.12 and 3.13 show the attenuation of the recorded CAP signal with the pressure exerted on the nerve. This may be due to the fact that the ion channels in the membranes of the nerve cells cannot function properly due to

the pressure exerted on the nerve. The aforementioned voltage source-induced noise is an important factor limiting the success of our system. In order to overcome this, appropriate filters should be developed.

With this study, we have successfully demonstrated that we can compress the sciatic nerve to the desired extent gradually and achieve this with current dynamic current control. We also proved that we can produce an electrode on a scale that can be implanted.

# 5. CONCLUSION

The aim of this study is to prove that a FINE electrode design can be used to gradually tighten the nerve and this design can be miniaturized enough to be implanted in the body. In the light of the data obtained, we can clearly say that the actuation mechanism we have designed has a function that can be used in the body and it has been shown by tests that it does not encounter any problems in applying pressure gradually to the nerve.

Characterization based on temperature determination in the electrode movement mechanism could not be carried out in accordance with the possibilities. However, this is a design that can be transformed into a commercial product if sufficient characterization is made.

In future work, the force generated by changes in spring production can be optimized. The electrode structure can be completely embedded in the silicone, thereby increasing the electrode tissue fit. This mechanism can be used not only in the shaping of the nerve, but also in studies of controlled damage to the nerve.

# REFERENCES


1. Corporation, M., "Introduction to Nitinol," *Memry Corporation*, Vol. 62, no. 2, 2017.

2. Abuzaiter, A., E. L. Ng, S. Kazi, and M. S. Mohamed Ali, "Development of Miniature Stewart Platform Using TiNiCu Shape-Memory-Alloy Actuators," *Advances in Materials Science and Engineering*, Vol. 2015, pp. 1–9, 2015.

3. Antonucci, V., and A. Martone, "Phenomenology of Shape Memory Alloys," in *Shape Memory Alloy Engineering*, pp. 33–56, Elsevier, 2015.

4. Wang, B., and S. Zhu, "Seismic behavior of self-centering reinforced concrete wall enabled by superelastic shape memory alloy bars," *Bulletin of Earthquake Engineering*, Vol. 16, pp. 479–502, jan 2018.

5. Hu, J. W., and M.-H. Noh, "Seismic Response and Evaluation of SDOF Self-Centering Friction Damping Braces Subjected to Several Earthquake Ground Motions," *Advances in Materials Science and Engineering*, Vol. 2015, pp. 1–17, 2015.

6. O'Brien, B., W. Carroll, and M. Kelly, "Passivation of nitinol wire for vascular implantsâa demonstration of the benefits," *Biomaterials*, Vol. 23, pp. 1739–1748, apr 2002.

7. Zhang, D., Z. Zhang, Z. Zi, Y. Zhang, W. Zeng, and P. K Chu, "Fabrication of graded TiN coatings on nitinol occluders and effects on in vivo nickel release," *Bio-Medical Materials and Engineering*, Vol. 18, no. 6, pp. 387–393, 2008.

8. Speck, K. M., and A. C. Fraker, "Anodic Polarization Behavior of Ti-Ni and Ti-6A 1-4 V in Simulated Physiological Solutions," *Journal of Dental Research*, Vol. 59, pp. 1590–1595, oct 1980.

9. Kapoor, D., "Nitinol for Medical Applications: A Brief Introduction to the Properties and Processing of Nickel Titanium Shape Memory Alloys and their Use in Stents," *Johnson Matthey Technology Review*, Vol. 61, pp. 66–76, jan 2017.

10. Miková, L., S. Medvecká, B. M. Kelemen, F. Trebuña, and I. Virgala, "Application of Shape Memory Alooy (SMA) as Actuator," *Metalurgija*, Vol. 54, no. 1, pp. 169–172, 2015.

11. Kumar, P., and D. Lagoudas, "Introduction to Shape Memory Alloys," in *Shape Memory Alloys*, Vol. 1, pp. 1–51, Boston, MA: Springer US, jan 2008.

12. Ishii, T., "Design of shape memory alloy (SMA) coil springs for actuator applications," in *Shape Memory and Superelastic Alloys: Technologies and Applications*, pp. 63–76, Elsevier, 2011.

13. Zhang, Y.-q., S.-y. Jiang, X.-m. Zhu, Y.-n. Zhao, Y.-l. Liang, and D. Sun, "Influence of Fe addition on phase transformation behavior of NiTi shape memory alloy," *Transactions of Nonferrous Metals Society of China*, Vol. 27, pp. 1580–1587, jul 2017.

14. Fernandes, D. J., R. V. Peres, A. M. Mendes, and C. N. Elias, "Understanding the Shape-Memory Alloys Used in Orthodontics," *ISRN Dentistry*, Vol. 2011, pp. 1–6, 2011.

15. ASTM Int., "Standard Test Method for Determination of Transformation Temperature of Nickel-Titanium Shape Memory Alloys by Bend and Free Recovery," tech. rep., 2016.

16. Rydevik, B., G. Lundborg, and U. Bagge, "Effects of graded compression on intraneural blood flow," *The Journal of Hand Surgery*, Vol. 6, pp. 3–12, jan 1981.

17. Lundborg, G., C. Nordborg, B. Rydevik, and Y. Olsson, "The Effect of Ischemia on the permeability of the Perineurium to Protein Tracers in Rabbit Tibial Nerve," *Acta Neurologica Scandinavica*, Vol. 49, pp. 287–294, jan 1973.

18. Gao, Y. M., C. S. Weng, and X. L. Wang, "Changes in nerve microcirculation following peripheral nerve compression," *Neural Regeneration Research*, Vol. 8, no. 11, pp. 1041–1047, 2013.

19. Borschel, G. H., K. F. Kia, W. M. Kuzon, and R. G. Dennis, "Mechanical properties of acellular peripheral nerve," *Journal of Surgical Research*, Vol. 114, pp. 133–139, oct 2003.

20. Janmey, P. A., J. P. Winer, M. E. Murray, and Q. Wen, "The hard life of soft cells," *Cell Motility and the Cytoskeleton*, Vol. 66, pp. 597–605, aug 2009.

21. Polikov, V. S., P. A. Tresco, and W. M. Reichert, "Response of brain tissue to chronically implanted neural electrodes," *Journal of Neuroscience Methods*, Vol. 148, pp. 1–18, oct 2005.

22. Xue, N., T. Sun, W. M. Tsang, I. Delgado-Martinez, S.-H. Lee, S. Sheshadri, Z. Xiang, S. Merugu, Y. Gu, S.-C. Yen, and N. V. Thakor, "Polymeric C-shaped cuff electrode for recording of peripheral nerve signal," *Sensors and Actuators B: Chemical*, Vol. 210, pp. 640–648, apr 2015.

23. Lee, S., S.-C. Yen, L.-D. Liao, G. G. L. Gammad, N. V. Thakor, and C. Lee, "Flexible sling electrode for bidirectional neural signal recording and selective stimulation," in *2016 IEEE 29th International Conference on Micro Electro Mechanical Systems (MEMS)*, Vol. 2016-Febru, pp. 375–378, IEEE, jan 2016.

24. Yu, H., W. Xiong, H. Zhang, W. Wang, and Z. Li, "A Parylene Self-Locking Cuff Electrode for Peripheral Nerve Stimulation and Recording," *Journal of Microelectromechanical Systems*, Vol. 23, pp. 1025–1035, oct 2014.

25. Park, D.-W., A. A. Schendel, S. Mikael, S. K. Brodnick, T. J. Richner, J. P. Ness, M. R. Hayat, F. Atry, S. T. Frye, R. Pashaie, S. Thongpang, Z. Ma, and J. C. Williams, "Graphene-based carbon-layered electrode array technology for neural imaging and optogenetic applications," *Nature Communications*, Vol. 5, p. 5258, dec 2014.

26. Blau, A., A. Murr, S. Wolff, E. Sernagor, P. Medini, G. Iurilli, C. Ziegler, and F. Benfenati, "Flexible, all-polymer microelectrode arrays for the capture of cardiac and neuronal signals," *Biomaterials*, Vol. 32, pp. 1778–1786, mar 2011.

27. Freeberg, M. J., M. A. Stone, R. J. Triolo, and D. J. Tyler, "The design of and chronic tissue response to a composite nerve electrode with patterned stiffness," *Journal of Neural Engineering*, Vol. 14, p. 036022, jun 2017.

28. Heo, D. N., S.-J. Song, H.-J. Kim, Y. J. Lee, W.-K. Ko, S. J. Lee, D. Lee, S. J. Park, L. G. Zhang, J. Y. Kang, S. H. Do, S. H. Lee, and I. K. Kwon, "Multifunctional hydrogel coatings on the surface of neural cuff electrode for improving electrode-nerve tissue interfaces," *Acta Biomaterialia*, Vol. 39, pp. 25–33, jul 2016.